

**Validation of rain rate estimation in hurricanes from the Stepped Frequency  
Microwave Radiometer: algorithm correction and error analysis**

By

Haiyan Jiang\*

Department of Meteorology

University of Utah, Salt Lake City, Utah

Peter G. Black

NOAA/Atlantic Oceanographic and Meteorological Laboratory

Hurricane Research Division, Miami, Florida

Edward J. Zipser

Department of Meteorology

University of Utah, Salt Lake City, Utah

Frank D. Marks, Jr. and Eric W. Uhlhorn

NOAA/Atlantic Oceanographic and Meteorological Laboratory

Hurricane Research Division, Miami, FL

Manuscript Submitted to *Journal of the Atmospheric Sciences*: Dec. 2003

Revised: Aug. 2004

\**Corresponding Author*: Haiyan Jiang, Department of Meteorology University of Utah, Salt Lake City,  
Utah 84112; E-mail: [hjiang@met.utah.edu](mailto:hjiang@met.utah.edu)

## Abstract

Simultaneous observations by the Lower Fuselage (LF) radar, the tail (TA) radar, and the Stepped Frequency Microwave Radiometer (SFMR) on board the National Oceanic and Atmospheric Administration (NOAA) WP-3D aircraft are used to validate the rainfall rate estimates from microwave emission measurements of SFMR in tropical cyclones. Data collected in Hurricane Bonnie (1998) and Hurricane Humberto (2001) with a total of 820 paired samples are used in the comparisons. The SFMR 10-s path-integrated rain rates are found to have an overestimate in light rain and an underestimate in heavy rain relative to radar rainfall estimates. Examination of the existing SFMR algorithm shows that the coefficient should be changed in the attenuation — rain rate relationship used in the inversion algorithm. After this correction, a linear regression result with a correlation coefficient of 0.8 and a slope close to 1 is obtained. But an overall high bias of  $5 \text{ mm h}^{-1}$  of the SFMR rainfall estimate relative to radar is also found. The error analysis shows that the bias is nearly independent of rain type, a result confirming Jorgensen and Willis's (1982) conclusion that the drop size distributions between convective and stratiform rain in hurricanes are similar. It is also shown that the bias is a weak function of wind speed, as well as a weak inverse function of radial distance to the hurricane center. We are able to rule out temperature dependence as the main explanation. After doing sensitivity tests, we conclude that the bias results from a combination of two factors: an underestimate of the freezing level height, and a downward increase of radar reflectivity in the high wind regions. If the true downward increase is  $1\text{-}2 \text{ dBZ km}^{-1}$  (c.f. Ferreira et al. 2001), a  $0.5 \text{ km}$  underestimate of the freezing level height could account for up to  $3\text{-}5 \text{ mm h}^{-1}$  bias.

## 1. Introduction

Accurate quantitative precipitation estimates within tropical cyclones over oceans represents a challenging problem. Obviously, no surface rain gauge data are available. Research aircraft can fly through the storm and provide precipitation estimates from passive and active instruments. This paper describes the validation of path-integrated rain rates from the Hurricane Research Division's (HRD) Stepped-Frequency Microwave Radiometer (SFMR). The SFMR is designed for the measurement of the sea surface wind speed and path-integrated rain rate. On board the NOAA WP-3D hurricane research aircraft, SFMR data are obtained on tropical cyclones over Atlantic Ocean during the NOAA HRD's annual program of research flights since 1980. Since 1999, the HRD began to transmit the real-time SFMR surface winds and rainfall rates to the Tropical Prediction Center (TPC) for application to hurricane forecasts. The advantage of SFMR is that it can potentially provide along aircraft track mapping of rain rates and surface wind speeds in high temporal resolution (1 Hz). The SFMR-derived surface wind is one of the most important data sources of direct hurricane inner-core surface wind speed estimates available for TPC forecasters (Black et al. 2000). The SFMR surface wind estimates have been well validated by Global Positioning System (GPS) dropwindsonde measurements (Uhlhorn and Black 2003; Black et al. 2000) and have been universally accepted. It is very important for hurricane forecasters to get the real-time, relatively accurate rain rate data matched with the surface wind speed data. In this paper, SFMR rain rates are compared with airborne radar data from two independent hurricane cases.

It has been long known that microwave attenuation  $K$  by rainfall is strongly correlated with rain rate  $R$  (Ryde 1947; Wexler and Atlas 1963; Olsen et al. 1978). But a specific  $K$ - $R$  relationship depends on the frequency, raindrop size distribution (DSD), and temperature (Olsen

et al. 1978). As more understanding on the K-R relationship was achieved, the SFMR rain algorithm was incrementally improved. The first experimental SFMR rain rate measurements were made in Hurricane Allen in 1980 by the first SFMR instrument built by the National Aeronautics and Space Administration's (NASA) Langley Research Center in 1978 (Harrington 1980). Four selectable frequencies between 4.5 and 7.2 GHz were used to produce a "stepping" procedure allowed for estimating the rain rate and wind speed. The first SFMR rainfall algorithm applied in Hurricane Allen (1980) data was developed and reported by Jones et al. (1981). By neglecting the effect of absorption by oxygen molecules, water vapor and nonprecipitating liquid water, the radiative transfer equation was solved to get the rain opacity  $\tau$ , which can be related to K and the depth of the rain column  $h$  by  $\tau = \exp(-Kh)$ , neglecting the effect of scattering at SFMR frequencies.  $\tau$  was further related to rain rate R by a linear relationship at a frequency of 6.6 GHz:  $R = 320\tau$ . The value 320 was chosen empirically. Agreement between airborne radar and SFMR estimates for a pass of Hurricane Allen was found to be within a factor of 2. Black and Swift (1984) refined the SFMR rain algorithm by a physically-based derivation of the attenuation coefficient K. Using brightness temperature measurements from two frequencies, K can be calculated iteratively. Applying a rain rate and frequency dependent power relationship between K and R derived by Olsen et al. (1978), SFMR rain rate was retrieved in a relatively good agreement with radar measurements. Despite the preliminary success in Allen, this original instrument was never again flown into a hurricane.

A new retrieval algorithm was implemented (Tanner et al. 1987; Uhlhorn and Black 2003) with the advent of a second SFMR designed and built in 1982 (Swift et al. 1986). With 6 frequencies instead of 4 between 4.5 and 7.2 GHz used in the new SFMR, an inversion technique was developed to infer two parameters (wind speed and rain rate) from six brightness

temperature measurements by using a microwave radiative transfer model. The second SFMR was also improved in hardware in the following decade by setting up a new antenna, upgrading the receiver so that an improved spatial resolution and a stable calibration are gained. Since 1980, the SFMR has flown on 95 flights in 30 tropical cyclones (Uhlhorn and Black 2003).

The airborne radar has proven its ability in estimating rainfall in hurricanes. Jorgensen and Willis (1982) derived an overall Z-R relationship from three mature hurricanes by using airborne disdrometer data and argued that this relationship could be used in both stratiform and convective rain regions of tropical cyclones without obvious bias. Marks (1985) used airborne radar to investigate the evolution of precipitation structure of Hurricane Allen (1980). In this study, the SFMR rain rate measurements in tropical cyclones are evaluated against airborne radar data. The radar data used here are from the Lower Fuselage (LF) radar and the tail (TA) radar on the NOAA WP-3D aircraft.

The quality of validation is dependent on the quality of the validation data. The task of accurately quantifying radar-rainfall has proven to be difficult. The reasons are threefold: 1) Despite Jorgensen and Willis' (1982) result, the Z-R relationship depends on the DSD that may vary from storm to storm or even from one part of a storm to another (Smith et al. 2001); 2) The LF radar has a large vertical beam width ( $4.1^\circ$ ), therefore a beamfilling problem (Amayenc et al. 1993; Baeck and Smith 1998; Durden et al. 1998); 3) The radar calibration could be a problem (Klazura et al. 1999). Based on this understanding, we carefully choose two mature hurricane cases (Bonnie 1998 and Humberto 2001) so that Jorgensen and Willis's (1982) overall Z-R relationship can be approximately applied assuming that the DSD variation in mature hurricanes is not very large. A near optimal comparison scheme is used to assure that the beamfilling problem is minimized from the LF radar. The effect of different sample volumes among these

three instruments, which are different by several orders of magnitude, is believed to be minimized by our data averaging and interpolating processes. This scheme also minimizes the attenuation effects and bright band contamination. It is well-known that LF and TA radars have suffered from calibration problems for years. Marks et al. (1993) found an 8.2 dBZ calibration error for LF radar during Hurricane Anita (1977). In this study, reflectivity measurements from a well-calibrated radar (ER-2 Doppler radar) are used to estimate the offsets of LF and TA radar reflectivity (see appendix).

The objectives of this study are 1) to establish a relatively accurate radar rain rate dataset collocated with SFMR observations to validate SFMR retrieval; 2) to refine the existing SFMR rain algorithm to improve its performance; 3) to quantitatively demonstrate that the rainfall estimated by SFMR now has the capability of serving as an important operational tool for mapping the distribution of precipitation in hurricanes; 4) to quantitatively describe the SFMR rain error in convective and stratiform precipitation, its dependence on storm parameters of interest, and direct possible future work based on the error analysis.

The following section describes the data sources (SFMR, LF, TA) used in this study, and the scheme developed to compare the three-dimensional radar data with one-dimensional (time series) SFMR data, and the procedures for interpolating the three data types so that they can match each other point by point. Comparison results and algorithm correction are presented in Section 3. Section 4 describes the error analysis. Sections 5 and 6 contain discussion and conclusions, respectively. The appendix is devoted to describing the calibration of the LF and TA radars.

## 2. Data sources and processing

### *a. SFMR data*

The HRD SFMR measures the microwave emissions from sea surface and intervening precipitation at six frequencies (4.55, 5.06, 5.64, 6.34, 6.96, 7.22 GHz) from its along-track nadir view. Since the antenna main beamwidth ranges from 22° to 32°, brightness temperatures at the six C-band channels can be obtained within footprints of 600~800 m depending upon the channel at a typical flight altitude of 1500 m (footprints would be larger if the flight altitude is higher). The hardware averaging time is set at 0.7-s, suggesting the theoretical single-measurement brightness temperature  $T_b$  resolution (noise) of  $\Delta T_b = 0.4$  K (Uhlhorn and Black 2003). The response time of the instrument is 0.85-s per channel. The time between completely independent sets of measurements is generally defined as twice the response, so the actual independent sampling time is  $2 \times 6 \text{ channels} \times 0.85\text{-s per channel} = 10\text{-s}$  (Uhlhorn and Black 2003).

Since rain is weakly attenuating at these microwave frequencies and the attenuation by rain is a function of electromagnetic wavelength, the frequency-stepping ability of the instrument suggests a procedure for retrieving the rain rate. Because the small ratio of the raindrop diameter (< 6 mm) to the SFMR wavelength (~ 5 cm), the radiative interaction of raindrops is mostly in the Rayleigh limit (some of big raindrops could be in Mie regime). According to Stephens (1994), in the Rayleigh regime the absorption cross section is proportional to  $D^3$  ( $D$  is the diameter of the raindrop), while the scattering cross section is proportional to  $D^6$ . Therefore for small raindrops, the absorption coefficient is much larger than the scattering coefficient. So the scattering effect can be neglected. A forward radiative transfer model was built by previous studies (Jones et al. 1981, Black and Swift 1984, Uhlhorn and Black 2003) by approximating an absorption process of rain. Given a physical model that relates the attenuation coefficient  $K$  to

measurements of  $T_b$  at several frequencies and a relationship between rain rate  $R$  and  $K$ , a set of simultaneous equations may be inverted to calculate the rain rate under practically all weather conditions (See appendix A of Uhlhorn and Black 2003 for a detailed description of the SFMR algorithm).

A theoretical noise level of SFMR single-measurement  $T_b$  is about 0.4 K (Uhlhorn and Black 2003). For rain rate less than  $5 \text{ mm h}^{-1}$ , the sensitivity of changes in the  $T_b$  to changes in rain rate at SFMR frequencies and nadir incidence angle is so weak that it is lost to its noise, and a solution is normally not possible. The minimum retrievable surface wind speed is  $10 \text{ m s}^{-1}$ . The SFMR algorithm is only suitable for measurements over ocean. It recognizes measurements entirely over land by a  $T_b$  threshold of 280 K. But when the antenna beam is partially filled by land, false rain rate retrieval can occur. In this comparison, rain rates  $< 5 \text{ mm h}^{-1}$  or measurements within 10 km of land are not included.

The algorithm outputs a rain rate estimate from the set of SFMR  $T_b$  measured at a rate of 1 Hz, but truly independent measurements are possible only at a slower sampling rate of 0.1 Hz, corresponding to a 10-s temporal resolution. For comparison with the airborne radar rain rate, a 10-s average SFMR value is calculated. Each of the independent variables (time and location) is adjusted to correspond to the averaged rain rate value.

#### *b. TA radar data*

The tail (TA) radar installed on the N43RF aircraft is a vertical scanning X-band (3.22 cm) radar with Doppler capability. It has a vertical beamwidth of  $1.9^\circ$  and a horizontal beamwidth of  $1.35^\circ$ . The spatial resolution along any radial ray is 75 m. The antenna, located in the tail of the aircraft, sweeps through the azimuth angles of  $0^\circ$  -  $360^\circ$  at an elevation angle of  $\pm 20^\circ$  relative to

the plane perpendicular to the aircraft ground track. Thus, the whole storm can be sampled by those vertical sweeps along the aircraft track, typically each 6-s at an aircraft ground speed of 100-120 m s<sup>-1</sup>.

The X-band radar is strongly affected by the attenuation from intervening precipitation particles. For minimizing the effect of attenuation, Marks (1985) constructed vertical time cross sections along the flight track and used only the radials pointing above and below the radar. In this comparison, only vertical cross section data from TA radar are included. Based on the vertical cross section image of TA reflectivity, rain type (stratiform/convective) is separated subjectively according to the bright band and local reflectivity gradient and maximum (Steiner et al. 1995).

Furthermore, during some hurricane seasons including 1998 and 2001, the French dual-beam antenna system was mounted on the N43RF TA radar. This antenna system carries two antennae, one pointing 20° forward and one pointing 20° aft. In the research fore-aft scanning mode, the radar transmitter has to switch from one antenna to the other after every sweep. The problem is that during this switch, the transmitter needs to be shut off for a few microseconds. The procedure usually affects the data quality for around nadir looking rays. In investigating the Bonnie and Humberto cases, we found that in the vertical time cross section constructed by using only the rays pointing above or below radar, the reflectivity is not continuous. Usually, the reflectivity values below the radar are much smaller than those above radar. This problem is probably a result of the transmitter switching. Therefore, we used the averaged radar reflectivity between the first bin above aircraft altitude (typically 1.5~2 km) and the bin at 3 km height toward the zenith to compare with SFMR along-track measurements. This averaged radar reflectivity is in 6-s temporal resolution along aircraft track. It is further interpolated into 10-s

resolution by a “nearest neighbor” method and converted into rain rate by using Jorgensen and Willis’ (1982) overall Z-R relationship:

$$Z = 300R^{1.35} \quad (1)$$

where  $Z$  is in  $\text{mm}^6 \text{ m}^{-3}$ ,  $R$  is in  $\text{mm h}^{-1}$ . This comparison is based on an assumption that in hurricane precipitation environment the vertical rain rate profile would keep nearly constant for the whole rain column, which is definitely not true. The error caused by this assumption will be discussed later.

*c. LF radar data*

The WP-3D C-band (5.59 cm) Lower Fuselage (LF) radar scans horizontally with a radial spatial resolution of 750 m. It has a vertical beamwidth of  $4.1^\circ$  and horizontal beamwidth of  $1.1^\circ$  (see the appendix of Jorgensen 1984 for details). Its purpose is to provide the plain view of the radar structure of tropical cyclones. A single sweep of the LF radar takes about 30-s. But the major problems of LF radar are 1) sea clutter contamination, 2) inadequate beamfilling, and 3) attenuation by intervening precipitation. The first two problems are mainly produced by the wide vertical beamwidth and antenna side lobes. Usually, the sea clutter problem could be minimized by lifting the elevation angle during radar operation. Marks (1985) gave a quantitative estimation of the mean signal loss caused by the inadequate beamfilling problem of LF. They showed that at an altitude of 1500 m, the mean loss is about 5 dB at the range of 100 km from radar, and increases up to 30 dB at the range of 300 km from radar. They also showed that typical losses as a result of rain attenuation for a wavelength of 5.5 cm are about half those caused by the inadequate beamfilling problem. They developed a technique to minimize these two effects by mapping time composites rather than a single sweep.

For comparing with SFMR along-track measurements, the LF data used here is from averaging the reflectivities on the bins of  $\pm 5^\circ$  around the direction of the flight track on the range of 7 km away from the airplane. Therefore we get one mean reflectivity value for a single sweep, bringing a temporal resolution of about 30-s since the antenna rotates twice a minute. We choose data at 7 km away from radar because 1) it is close enough to radar so that the sea clutter, inadequate beamfilling, and attenuation problem will be negligible in most cases; 2) it is far away enough from radar to avoid the first several bins from radar which are contaminated; 3) at the usual elevation angle of  $3^\circ - 4^\circ$ , at 7 km range, the beam is 0.4 km above the radar altitude, a level of about 2~2.5 km above sea level. This averaged LF reflectivity at 2~2.5 km altitude is interpolated into 10-s temporal resolution and converted into rain rate value similar as what has been done for TA data. The LF data mapping is comparable with the scheme for TA data (section 2b), assuring no bright band contamination.

### **3. Comparison results and algorithm correction**

A total of 820 paired samples of SFMR and airborne radar rain rates were obtained from Hurricane Bonnie and Humberto on Aug. 24 & 26, 1998 and on Sep. 23 & 24, 2001 respectively (see table 1 for a detailed summary of flights). The flight altitudes ranged from 1.5 to 2.1 km and each of the four flights sampled mature hurricanes with SFMR maximum wind above  $34 \text{ m s}^{-1}$ . To be included, the measurements had to be in a rain region based on the TA radar vertical cross section image. A minimum rain rate of  $5 \text{ mm h}^{-1}$  was thresholded for both SFMR and radar observations. The geographic locations of SFMR/radar co-located rain rate measurements are plotted in Fig. 1 including flight tracks and storm centers during the time period of paired samples. All of the four flights included storm inner core region sampling. The classification of

rain type has been done subjectively by examining the TA vertical cross section of reflectivity. A total of 563 (69%) paired samples were classified as stratiform; while 257 (31%) samples as convective. This classification has more convective points than the climatological average in hurricanes (Cecil et al, 2002). This oversampling of heavy rain regions in the 820 data samples is an expected result because of our eliminating rain rates less than  $5 \text{ mm h}^{-1}$ .

*a. Regression analysis*

The scatterplots of SFMR versus LF and TA rain rates for all 820 paired samples are shown in Fig. 2. A high correlation between SFMR and radar measurements is shown by the correlation coefficients of 0.82 for SFMR relative to both LF and TA. But the slopes of the least squares best fits of 0.60 (SFMR vs. LF) and 0.65 (SFMR vs. TA) represent an overestimate of SFMR rain retrievals for rain less than  $10 \text{ mm h}^{-1}$  and an underestimate for rain greater than  $10 \text{ mm h}^{-1}$ . This result is from the comparison with two independent sets of radar measurements. For independent storm cases and different rain types, the same tendency can be seen from the regression results. Table 2 gives the comparison of correlation coefficients and best fit equations of SFMR versus LF and TA rain rates for all samples, Bonnie only, Humberto only, stratiform only, and convective only. Although a small range of variation among those fitting parameters of subsets of samples, the systematically low slopes and high intercepts are obvious. The slope of best fit ranges from 0.54 to 0.68, while the intercept ranges from 3.73 to  $6.88 \text{ mm h}^{-1}$ . Generally the regression equations have greater slope and smaller intercept between SFMR and TA than those between SFMR and LF. This better agreement with the TA radar will be discussed later.

### *b. Algorithm correction*

As described in appendix A (b) of Uhlhorn and Black (2003), the SFMR rain algorithm used the following empirical relationship between the rainfall attenuation coefficient  $K$  and rain rate  $R$ :

$$K = aR^b \quad (2)$$

where  $K$  is in  $\text{Np km}^{-1}$  ( $1 \text{ Np} = 4.34 \text{ dB}$ ),  $R$  is in  $\text{mm h}^{-1}$ ;  $a$  and  $b$  are empirical parameters. Olsen et al. (1987) have shown that  $a$  is a function of  $R$  and frequency  $f$ :

$$a = gf^{n(R)} \quad (3)$$

It has been shown that  $n \approx 2.6R^{0.0736}$  (Atlas and Ulbrich, 1977) and  $g = 1.87 \times 10^6 \text{ Np km}^{-1}$  (Black and Swift, 1984). In the SFMR algorithm used here, the exponent  $b$  was taken to be 1.35 according to Jorgensen and Willis (1982). *In fact,  $b = 1.35$  is for the empirical radar reflectivity  $Z$ - $R$  instead of  $K$ - $R$  relationship in hurricanes.* As given by Willis and Jorgensen (1981) from aircraft microphysics observations of three mature hurricanes, the empirical relation derived between C-band radar reflectivity factor  $Z$  and attenuation coefficient  $K$  is:

$$K = 9.78 \times 10^6 Z^{0.85} \text{ (dB km}^{-1}\text{)} \quad (4)$$

Combining (1) and (4), we get the exponent of the empirical  $K$ - $R$  relation  $b = 1.35 \times 0.85 = 1.15$ . After running Mie calculations based on the hurricane DSD provided by Merceret (1974), we found that the exponent of the “theoretical”  $K$ - $R$  relationship is also 1.15 at 6.6 GHz and ranges from 1.10 to 1.18 at 4.55-7.22 GHz.

A similar plot as Fig. A3 of Uhlhorn and Black (2003) but with a new value of exponent  $b=1.15$  is given in Fig. 3, showing the rainfall attenuation coefficient  $K$  as a function of rain rate. This new parameter of  $b$  brings a big change in the SFMR rain retrieval. Table 3 lists the comparison of original SFMR retrieved and  $b$ -coefficient corrected SFMR rain rates at a set of

K values at the highest frequency (7.22 GHz) of SFMR. Typically, the differences between original and corrected rain rates increase with rain intensity, reflecting a decreasing of  $b$  coefficient in (4). For example, an original retrieved rain rate of  $5 \text{ mm h}^{-1}$  corresponds to a corrected one of  $6.13 \text{ mm h}^{-1}$ , which is the new minimum retrievable rain rate value of SFMR; while an original retrieved  $50 \text{ mm h}^{-1}$  corresponds to a corrected  $80 \text{ mm h}^{-1}$ . This correction directly addresses the relative insensitivity problem of the old SFMR rainfall algorithm discussed in section 3a.

After rerunning the SFMR retrieval program for the entire two storms dataset by adding a  $b$ -coefficient correction, the new linear regression result for all samples is given in Fig. 4. The new minimum retrievable rain rate is  $6.13 \text{ mm h}^{-1}$ , but the rain threshold in Fig. 4 is not changed from the original  $5 \text{ mm h}^{-1}$  threshold since it does not make any difference on the regression results. As expected, the new slope of least squares fit to the data is close to 1 for both SFMR versus LF and SFMR versus TA. The correlation coefficient remains unchanged, but generally, the SFMR rain rate is overestimated relative to radar measurement at a magnitude of  $5 \text{ mm h}^{-1}$  as indicated by the mean error. The overestimation is nearly independent of magnitude. Similarly as in Table 2, Table 4 shows mean errors and least square best fit equations of corrected SFMR versus LF and TA rain rates for different storms and different rain types. Correlation coefficients are not listed because they are as same as those in Table 2. Again, no important difference is found. However, SFMR versus LF regressions still represent a greater disagreement, with slopes down to 0.85, intercept up to 8.33, and mean bias high up to 6.91.

The PDFs and CDFs of the distribution of errors, defined as SFMR minus LF and SFMR minus TA, are plotted in Fig. 5. Both PDFs peak at a positive value of  $3\sim 5 \text{ mm h}^{-1}$ , revealing an

overestimation of SFMR. The CDFs indicate that the middle 50% of the errors range between approximately 0 and + 6 mm h<sup>-1</sup>.

Now we explain the difference between TA and LF rain rate estimates compared with SFMR. Referring to Table 2, 4 and Fig. 2, 4, 5, some difference still exists between SFMR versus TA and SFMR versus LF. In general, the mean errors between SFMR and TA are less than those between SFMR and LF. The slopes of best fit for SFMR versus TA are closer to 1 for both “all” samples and four sub-samples (Table 4), although correlation coefficients remain similar for both comparisons (Table 2). From the CDFs of SFMR errors (Fig. 5), for most percentiles, SFMR minus LF is larger than SFMR minus TA by about 0.2~0.4 mm h<sup>-1</sup>. This is also indicated by mean errors shown in Fig. 5. The systematic difference is not surprising if we consider the different data processing scheme for three instruments (section 2) for obtaining matched observations. The field of view among SFMR, TA, and LF are very different. As mentioned in section 2, SFMR looks the whole rain column from the freezing level to the sea surface. The TA radar data are sampled from upward looking bins from aircraft altitude up to 3 km, while the LF data are sampled from bins 7 km ahead the aircraft and 10 azimuth degrees averaging from left to right of the aircraft track. It is believed that TA data is more comparable with SFMR because both of their data samples are taken from the vertical column of rain and the vertical path-integrated rain rate, which might be very different from the horizontally averaged rain rate. So for simplicity, we focus only on SFMR minus TA as the error of SFMR rain estimate in the following section of error analysis.

#### 4. Error analysis

To improve our understanding of how the error distribution is related to some hurricane parameters of interest, this section is devoted to investigate the rain type dependence, wind speed dependence, and radial distance dependence of errors.

##### *a. Rain type dependence of errors*

It is still an open question how much variation in DSD may occur in hurricanes and whether there is any systematic difference between rain types. Here we use the results of section 3 to investigate this question for our database.

As noted in section 3, there is a different regression result for stratiform and convective samples. Fig. 6 gives PDFs and CDFs of SFMR rain rate errors (SFMR minus TA) for these two subsets. The standard deviation is  $5.7 \text{ mm h}^{-1}$  ( $3.6 \text{ mm h}^{-1}$ ) for convective (stratiform) rain. It is not just the DSD that is more variable; any slight mismatch in the sample volumes will give variation in convective regions, because almost by definition, horizontal variability in rain rate is higher at smaller scales. The PDF of errors for stratiform samples peaks at  $3 \text{ mm h}^{-1}$ , while the PDF for convective samples has two peaks, one is at  $-1 \text{ mm h}^{-1}$ , another is at  $+4 \text{ mm h}^{-1}$ . This also shows the DSD variation and the effect of beam mismatching in convective regions.

Although the effect of DSD variation on K-R relation can be seen clearly within convective regions, the mean error in convective rain ( $5.32 \text{ mm h}^{-1}$ ) is only slightly larger than that in stratiform rain ( $4.48 \text{ mm h}^{-1}$ ), a result showing that there is only a weak dependence of the average K-R relation on rain type or DSD. This fact verifies that a separation of K-R relation for different rain type would not produce significant difference on the SFMR rain estimate.

Although from the regression for all samples there is no error dependence on rain intensity, the SFMR error as a function of TA radar rain rate is investigated for stratiform and convective samples respectively (Fig. 7). Again, only a very weak dependence is found from Fig. 7, that is, the SFMR error for stratiform precipitation increases slightly with rain rate, but the reverse is the case for convective precipitation.

*b. Wind speed dependence of errors*

The SFMR can estimate surface wind as well. Rain rate and wind speed are retrieved at the same time from the SFMR inversion algorithm, and Uhlhorn and Black (2003) reported an overall bias of  $2\sim 3 \text{ m s}^{-1}$  of SFMR wind estimates relative to GPS 10-m winds. Although it was shown that this bias is independent of wind speed, we ask whether this kind of independence exists for the SFMR rain error as well.

The SFMR rain errors, again defined here as SFMR minus TA, are plotted as a function of the SFMR wind speed in Fig. 8 for stratiform and convective separately. Here the SFMR wind speed is recalculated after the  $b$ -coefficient correction because the SFMR wind retrieval depends on the rain retrieval. A weak increase is seen in the SFMR's overestimation with increased SFMR surface wind for both rain types. The correlation coefficients are 0.29 for 563 stratiform samples and 0.34 for 257 convective samples respectively. Because the SFMR wind is retrieved by relating it to the excess emissivity of wind-driven sea relative to specular emissivity of tropical ocean, it is highly possible that in high wind regions, the wind-emissivity model is biased, therefore producing biased rain rates. From the regressions in Fig. 8, this wind effect tends to influence convective regions more than stratiform regions, but the difference may not be significant.

### *c. Radial dependence of errors*

Rainfall, wind speed, and temperature in a hurricane are generally a function of radial distance  $r$  from the center. To find out the radial dependence of SFMR errors, the data have been analyzed according to their normalized radial distance, defined as  $r$  divided by the radius of maximum wind  $r_0$ . Hurricane spline fit storm track data from aircraft observations (Neal M. Dorst, personal communication) is used to get  $r$  for each sample. For each radial tranverse,  $r_0$  is identified from the SFMR data. A mean of these  $r_0$  for each storm is used to normalize  $r$ .

Fig. 9 plots the SFMR error as a function of normalized radial distance. All data used in this study were sampled within  $r/r_0 = 4$ . A decrease is obvious in SFMR error with increased distance from the storm center for both precipitation types. The correlation coefficients are 0.46 and 0.50 respectively. The similarity between correlation coefficients in Fig. 8 and Fig. 9 suggests that 1) there is no important difference of the error dependences for different rain types; 2) the radial dependence of SFMR error may simply reflect the wind error. The temperature dependence on radius was also considered. Although the SFMR wind speed retrieval is not sensitive to sea surface temperature as tested by Uhlhorn and Black (2003), the rain retrieval does depend on the average air temperature in the whole rain column because the temperature dependence of K-R relationship (Olsen et al. 1978). But the flight level temperature in our data set in most of the rain regions varies less than  $1 \sim 2^\circ C$ , which produces a 2% rain rate error. So we can rule out the effect of temperature variation as a significant factor.

## **5. Discussion**

This paper compares SFMR rain rates with radar measurements in a scheme for avoiding some limitations of airborne radar observations. In this scheme, the radar rain rate approximately

corresponds to an average rain rate at  $\sim 1.5\text{-}3$  km altitude<sup>1</sup>. Therefore, the radar rain rate used here is very close to the average rain rate in the whole rain column (from surface to the freezing level, about 0-4.5 km) if the vertical rain rate profile is approximately linear, either constant or increasing or decreasing downward. As mentioned at the end of section 3, here we still only talk about the TA radar. The data sampling scheme of LF is similar to that of TA.

The SFMR senses not only the upward emission from the aircraft down to the sea surface, but also the downwelling microwave radiation from the sea surface up to the freezing level. The SFMR algorithm takes these two contributions into account by assuming a constant rain rate from the freezing level to the sea surface. Therefore, the SFMR-retrieved rain rate is supposed to represent the path integrated (averaged) rain rate along the whole rain column. However, whether this is true depends upon the true shape of the rain rate vertical profile, because the weighting factors of the radiative contributions from the rain column above and below the aircraft are different. They are a function of the atmospheric temperature profile. Therefore the effect of the shape of the rain rate profile could cause some bias of the SFMR rain relative to the radar rain.

As an emission/attenuation-based rainfall algorithm (Wilheit 1977), the SFMR retrieval could be sensitive to the freezing level height assumption because the radiation received by the SFMR is directly related to the rain layer thickness. One might also be concerned about the effect of the presence of the non-precipitating cloud liquid water content on the SFMR rain rate retrieval. A sensitivity test is performed by adding cloud liquid water content in an assumed amount of 20% of the rain water content. This is about the maximum percentage in the hurricane environment according to three-dimensional cloud resolving model results. The sensitivity test

---

<sup>1</sup> The aircraft altitude can be 1.5 or 2 km, in the following text,  $\sim 1.5\text{-}3$  km will be used for simplicity.

shows the SFMR rain rate retrieval would change by only about an average of 0.5% for this large amount of cloud liquid water content.

The sensitivity tests of the SFMR-retrieved rain rate to the shape of the vertical profile of rain rate and to the uncertainty of the freezing level height have been performed. The idealized SFMR brightness temperature data are set up as follow. The shape of the rain rate profile is varied setting a  $\pm 5 \text{ mm h}^{-1}$  difference between the mean rain rate above the aircraft (*rain\_above*) and that below the aircraft (*rain\_below*). In the original SFMR algorithm, a fixed 4 km freezing level height is assumed for all storms. By checking the TA radar bright band height, we found that the true average freezing level heights for Bonnie and Humberto are 4.8 and 4.3 km, respectively. Here we use 4.5 km to test the uncertainty relative to the original 4 km assumption. Fig. 10a presents the separate effect of the uncertainties in the vertical shape of the rain rate profile and the freezing level height. The SFMR-retrieved rain rate is plotted as a function of the true path-integrated (mean) rain rate over the whole rain column for 1) the freezing level = 4.5 km, 2)  $\text{rain\_above} = \text{rain\_below} - 5 \text{ mm h}^{-1}$ , 3)  $\text{rain\_above} = \text{rain\_below} + 5 \text{ mm h}^{-1}$ , respectively. In Fig. 10a, the 1:1 line corresponds to  $\text{rain\_above} = \text{rain\_below}$ . The retrieved rain rate is greater than the true mean for  $\text{rain\_above} = \text{rain\_below} - 5 \text{ mm h}^{-1}$ , with overall high bias about  $0.4 \text{ mm h}^{-1}$ . For  $\text{rain\_above} = \text{rain\_below} + 5 \text{ mm h}^{-1}$ , the retrieved mean rain rate is smaller than the true mean, with overall low bias about  $0.9 \text{ mm h}^{-1}$ . An obvious high bias of  $2.5 \text{ mm h}^{-1}$  results from the assumption of a freezing level height too low by 500 m.

Fig. 10b shows the combination effect of above two factors. For the freezing level = 4.5 km and  $\text{rain\_above} = \text{rain\_below} - 5 \text{ mm h}^{-1}$ , the overall high bias is about  $3.5 \text{ mm h}^{-1}$ ; for the freezing level = 4.5 km and  $\text{rain\_above} = \text{rain\_below} + 5 \text{ mm h}^{-1}$ , the overall high bias is about  $1.4 \text{ mm h}^{-1}$ .

In nature, the rain rate profile could be constant or increase downward or decrease downward in the whole rain column. Although it is still open to debate (Szoke and Zipser 1986, Zipser and Lutz 1994, Steiner et al. 1995, Yuter and Houze 1995, and Heymsfield et al 2000, etc), the shape of the vertical radar reflectivity profile in hurricanes has been investigated by some recent studies during the TRMM era. Ferreira et al (2001) used TRMM PR reflectivity profiles to test TRMM rainfall algorithms using two hurricane cases: Bonnie (1998) and Bret (1999). They showed the shape of PR standard algorithm 2A25 radar reflectivity profiles in these two storms in stratiform and convective regions. From the mean profiles for Bonnie (see their Fig. 4a and Fig. 5a), the reflectivity increases downward from the freezing level (4.8 km) to 1.5 km by 1 dB in stratiform rain regions and by 3~4 dB in convective rain regions. For Bret, their Fig. 14 showed a 0 dBZ increase in stratiform regions and a 3~5 dBZ increase downward in convective regions. Combining those results, a 2~3 dBZ increase downward from the freezing level to 1.5 km was given by Ferreira et al (2001) on average. Their results are consistent with the Cecil et al (2002) climatology from a 1-year TRMM hurricane database (see their Fig. 3), and the Heymsfield et al (2000) EDOP mean reflectivity profiles for two Bonnie passes (see their Fig. 9b). If we assume the slope of the vertical radar reflectivity profile is as same as the Ferreira et al (2001) result, then a 1~2 dBZ reflectivity increase for each 1.5 km altitude all the way down to surface is a reasonable estimate. The altitude difference between *rain\_below* and *rain\_above* is about 1.5 km. In the 820 samples used in this study, the mean LF and TA reflectivity is around 40 dBZ. By applying the Z-R relationship in (1), 1~2 dBZ reflectivity error at 40 dBZ corresponds to a rain rate error of 3~5 mm h<sup>-1</sup>. Therefore we tentatively conclude that on average, *rain\_below* is greater than *rain\_above* by about 3~5 mm h<sup>-1</sup>.

Based on the above estimate, the combination of the true freezing level being near 4.5 km and  $rain_{above} = rain_{below} - 5 \text{ mm h}^{-1}$  may explain our initial finding of the SFMR's high bias. According to Fig. 10b, with these assumptions, the overall high bias could be about 3.5 mm h<sup>-1</sup>. Back to Fig. 6, the mean SFMR error of 4.48 mm h<sup>-1</sup> for stratiform and 5.32 mm h<sup>-1</sup> in convective rain would be mostly canceled out if we take the uncertainty of the freezing level height and the shape of the vertical rain rate profile into account, leaving an uncertainty of  $\pm 2$  mm h<sup>-1</sup>.

The near independence of the K-R relation on precipitation types in hurricanes shown in this study is consistent with Jorgensen and Willis's (1982) result on the independence of Z-R relation on rain types. We understand that at the SFMR frequencies, K is approximately proportional to  $D^3$ , Z is proportional to  $D^6$ , and R is proportional to  $V(D)D^3$ .  $V(D)$  is the terminal fall velocity of raindrops, which is approximately proportional to  $D^{0.5}$  to  $D^1$  for raindrops and frozen hydrometeors depending on their sizes and habits, etc. (Rodgers and Yau 1989; Pruppacher and Klett, 1997). Therefore the DSD dependence of the K-R relation is supposed to be weaker than that of the Z-R relation, but it is still not totally independent in theory, especially in heavy rain regions where some large raindrops exists and the Rayleigh approximation is violated. So the overall independence on rain types for both Z-R and K-R relations must imply something about DSD in hurricanes. With the verification from two independent studies, one may conclude that the variation of DSD in hurricanes is relatively small, on average, between convective and stratiform rain types.

The variation of DSD and Z-R and K-R relations in different rain types has been studied extensively for many kinds of precipitation systems other than hurricanes. Stout and Mueller (1968) summarized that in radar rainfall estimate there are differences on the order of 150% that

can be attributed to different types of rain or different synoptic conditions. Delrieu et al. (2000) presented the K-R relation variations among “widespread”, “thunderstorm” and the intense long-lasting autumn rain events in Cevennes in France. Compared with the above studies, the conclusion of the near-independence of DSD on rain types in hurricanes in this study is paradoxical. But this apparent discrepancy could be explained by considering the special hurricane precipitation environment. By using airborne Doppler radar observations in Hurricane Alicia, Marks and Houze (1987) found that the precipitation particles advected from the upper levels of the eyewall by the radial flow are carried azimuthally as many as one-and-a-half times around the storm by the strong tangential flow of the vortex before they reach the melting level. Houze et al. (1992) called hurricane as a giant “mixmaster” that stirs and tends to homogenize the precipitation region lying just outside the eyewall. It is probable that the variation of DSD between convective and stratiform rain in hurricanes is minimized by the large horizontal wind, which is distinctly different from other rain systems. It is also extensively verified that the convective intensity in hurricanes and other tropical oceanic features is generally modest compared with precipitation features over continents (Jorgensen et al. 1985; Szoke et al 1986; Molinari et al. 1996; Black et al. 1996; Cecil and Zipser 2002; and Cecil et al. 2002;). In these studies, even in the convective cases, the radar reflectivity profiles above the freezing level decrease rapidly with height and the updraft magnitudes are far less than that in continental convection. Therefore, the characteristics of convective rain in hurricanes may be somewhat similar to those in stratiform rain.

## 6. Conclusion

The passive microwave radiometer is a useful tool for measurement of path-integrated rain rates in hurricanes. The “path integrated” means that the SFMR senses the microwave emissions, and therefore brightness temperatures, from the whole rain column from the freezing level to the sea surface. The instrumentation of SFMR has an additional advantage that it will not saturate until a very high rain rate, unlike other radiometers with higher frequencies. The SFMR retrieved rain rates are well correlated with airborne radar rainfall measurements. After checking the algorithm carefully, the underestimate in high rain regions and overestimate in low rain regions of SFMR rain relative to radar observations have been removed by a  $b$ -coefficient correction. The SFMR provides independent estimates of rain rates at a horizontal resolution of  $\sim 10$ -s (1.5 km) along the flight track. The SFMR rainfall is another important measurement in hurricanes for operational applications.

An overall high bias ( $\sim 5 \text{ mm h}^{-1}$ ) of the SFMR rain rate estimates relative to radar was found. Based on the sensitivity tests, we can rule out the effect of the non-precipitating cloud liquid water, and the major reasons are the combination effect due to the uncertainty of the freezing level height and the shape of the vertical rain rate profile in hurricanes. An 0.5 km underestimate of the freezing level height can cause to  $3.5 \text{ mm h}^{-1}$  high bias of the SFMR rain if the true slope of vertical radar reflectivity is  $1\sim 2 \text{ dBZ per } 1.5 \text{ km}$  increasing downward (as in Ferreira et al. 2001). But one should be cautious since the radar reflectivity profile in the lowest 1.5 km is unknown for most radars because of ground clutter. Another factor to explain the SFMR high bias is the sensitivity of SFMR estimates to fractional coverage of the sea surface foam and spray. This is found by examining the dependence of SFMR rain error relative to radar on wind speed and normalized radial distance to the storm center.

Near-independence of SFMR rain errors on rain types is found. It is inferred that the K-R relation in hurricanes is similar for different precipitation types. Combined with Jorgensen and Willis' (1982) result of the independence of the Z-R relation on different rain types in hurricanes, this result supports the conclusion that the variation of DSD in hurricanes is small relative to other precipitation systems.

### **Appendix: Calibration of LF and TA radar**

The calibration of TA and LF radar can shift as a result of repairs, upgrades, and other factors. The general statement of the calibration error of TA and LF is as great as 5~6 dB (Oury et al. 1999, Marks et al. 1993), but it varies year by year due to major updates and repairs at the beginning of each hurricane season. As concluded by Atlas (2002), "After 56 years research in radar meteorology, we have still failed to find a reliable and universally applicable method of radar calibration." However, for individual applications, some successful calibration methods were developed. Marks et al. (1993) presented a method to calibrate LF radar by using the DSD measurement on aircraft during Hurricane Anita (1977). An 8.2 dB underestimate was found for LF radar during 1977 mission season.

Another way to determine the radar calibration error is to use a well-calibrated radar for comparison. The Tropical Rainfall Measurement Mission (TRMM) Precipitation Radar (PR) data have been used to calibrate ground-base radar data (Anagnostou et al. 2000; Bolen and Chandrasekar 2000; Schumacher and Houze 2000) because of the remarkable stability of PR. The NASA ER-2 Doppler radar (EDOP) has very stable characteristics, and it has been calibrated by the PR. The EDOP is an X-band (9.6 GHz) Doppler radar with fixed nadir and forward pointing beams with a beam width of  $2.9^\circ$ . It flies on the NASA ER-2 aircraft at 20 km

altitude and can map out the reflectivities and Doppler winds in the vertical plane along the aircraft path. A detailed description of the EDOP instrument can be found in Heymsfield et al. (1996). During the joint NASA/NOAA aircraft-based field programs into tropical cyclones in 1998 and 2001, a large volume of coordinated EDOP, TA and LF radar data were collected. Hurricane Bonnie (1998) and Humberto (2001) data are dealt with separately to find preliminary calibration estimates.

Two steps are involved in the preliminary TA and LF calibration estimate. Because both EDOP and TA obtain data in a vertical plane, we compare TA with EDOP in the first step by using along-track vertical cross section data. The second step is to obtain LF calibration estimate by comparing with corrected TA data. In the EDOP-TA comparison, reflectivity data above 2 km are used to minimize the attenuation effect for EDOP and to eliminate the “French Antenna” problem of TA (section 2b). During Bonnie flights, although there is no exactly matched flight pass between ER-2 and N43RF aircraft, a long time period of data sample (e.g. totally 5-hr flight for EDOP and 6-hr flight for TA) is recorded by both EDOP and TA during Aug. 24 & 26, 1998. By assuming the whole storm was sampled comparably by both radars in this long period flights, the histograms of EDOP and TA reflectivity in the along track vertical cross section above 2 km are compared. A +6 dB offset is found for TA reflectivity during Bonnie 1998. Figure A1 gives the comparison of probability density functions (PDFs) and cumulative density function (CDFs) of the EDOP reflectivity and TA corrected reflectivity (+6.0 dB). Except for the range of 0-6 dB, which is in no-rain region, a good agreement can be seen between EDOP and corrected TA data. The error analysis given in Table A1 shows that this +6.0 dBZ correction on TA reflectivity produces an error of  $\pm 1 \sim 2$  dB by comparing with EDOP CDFs. During Humberto (2001) flights, a nearly exactly matched leg is found around 21:40 UTC on Sep. 23. Comparing the

histograms of EDOP and TA reflectivity during this leg, a +4.5 dB offset is put on TA data for a preliminary calibration estimate. Figure A2 shows the comparison of PDFs and CDFs of EDOP and TA dBZs during this leg after shifting +4.5 dB for TA. There is a good agreement above 20 dBZ, but below that, the frequency difference may be caused by the small mismatch at the edge of this leg. The error analysis is also given in Table 1, showing an error within  $\pm 1 \sim 2$  dB after calibration, which is sufficient for the analyses of this paper.

LF is calibrated by comparing the LF and TA along-track averaged dBZ values. The along-track averaged dBZ data is produced by using the scheme described in Section 2. No calibration error is found for LF during the Bonnie mission, while a +6.5 dB offset is found for the Humberto mission.

### **Acknowledgements**

We are pleased to acknowledge Paul A. Leighton who processed LF and TA radar data for being used in this study. Funding has been provided by NASA CAMEX-4 grant NAG5-10682. We would like to thank Ramesh Kakar (NASA headquarters) for his continued support of CAMEX science. Thanks to Dr. Edward Walsh, Robert Black and Peter Dodge for useful discussions on this research. The constructive suggestions from 3 anonymous reviewers resulted in substantial improvements to the manuscript.

### **References**

- Amayenc, P., M. Marzoug, and J. Testud, 1993: Analysis of crossbeam resolution effects in rainfall rate profile retrieval from a spaceborne radar. *IEEE Trans.*, **GE-31**, 417–425.
- Anagnostou E. N., C. A. Morales, and T. Dinku, 2001: The use TRMM precipitation radar observations in determining ground radar calibration biases. *J. Atmos. Oceanic Technol.*, **18**, 616-628.

- Atlas, D., 2002: Radar calibration: some simple approaches. *Bull. Amer. Meteor. Soc.*, **83**, 1313-1316.
- \_\_\_\_\_, and C. W. Ulbrich, 1977: Path- and area-integrated rainfall measurement by microwave attenuation in the 1–3 cm band. *J. Appl. Meteor.*, **16**, 1322–1331.
- Baeck, M. L., and J. A. Smith, 1998: Rainfall estimation by the WSR-88D for heavy rainfall events. *Wea. Forecasting*, **13**, 416–436.
- Black, M. L., R. W. Burpee, and F. D. Marks Jr, 1996: Vertical motion characteristics of tropical cyclones determined with airborne Doppler radial velocity. *J. Atmos. Sci.*, **53**, 1887-1909.
- Black, P. G., and C. T. Swift, 1984: Airborne stepped frequency microwave radiometer measurements of rainfall rate and surface wind speed in hurricanes. Preprints, *22<sup>nd</sup> Conf. on Radar Meteorol.*, Zurich, Amer. Meteor. Soc., 433-438.
- \_\_\_\_\_, E. Uhlhorn, M. Powell, and J. Carswell, 2000: A new era in hurricane reconnaissance: real time measurement of surface wind structure and intensity via microwave remote sensing. Preprints, *24<sup>th</sup> Conf. Hurricane and Tropical Meteorology*, Ft. Lauderdale, FL, Amer. Meteor. Soc., 199-200.
- Bolen, S. M., and V. Chandrasekar, 2000: Quantitative cross validation of space-based and ground-based radar observations. *J. Appl. Meteor.*, **39**, 2071–2079.
- Cecil, D. J., and E. J. Zipser, 2002: Reflectivity, ice scattering, and lightning characteristics of hurricane eyewalls and rainbands. Part II: Intercomparison of observations. *Mon. Wea. Rev.*, **130**, 785-801.
- \_\_\_\_\_, \_\_\_\_\_, and S. W. Nesbitt, 2002: Reflectivity, ice scattering, and lightning characteristics of hurricane eyewalls and rainbands. Part I: Quantitative description. *Mon. Wea. Rev.*, **130**, 769-784.
- Delrieu, G., H. Andrieu, and J. D. Creutin, 2000: Quantification of path-integrated attenuation for X- and C-band weather radar systems operating in Mediterranean heavy rainfall. *J. Appl. Meteor.*, **39**, 840–850.
- Durden, S. L. Z. S. Haddad, A. Kitiyakara, and F. K. Li, 1998: Effects of nonuniform beam filling on rainfall retrieval for the TRMM precipitation radar. *J. Atmos. Oceanic Technol.*, **15**, 635–646.
- Ferreira, F., P. Amayenc, S. Oury, and J. Testud, 2001: Study and tests of improved rain estimates from the TRMM precipitation radar. *J. Appl. Meteor.*, **40**, 1878–1899.
- Harrington, R. F., 1980: The development of a stepped frequency microwave radiometer and its application to remote sensing of the earth. NASA Tech. Rep. TM-81847, 169 pp.

- Heymsfield, G. M., B. Geerts, and L. Tian, 2000: TRMM precipitation radar reflectivity profiles as compared with high-resolution airborne and ground-based radar measurements. *J. Appl. Meteor.*, **39**, 2080-2102.
- \_\_\_\_\_, S. W. Bidwell, I. J. Caylor, S. Ameen, S. Nicholson, W. Bonczyk, L. Miller, D. Vandemark, P. E. Racette, and L. R. Dod, 1996: The EDOP radar system on the high-altitude NASA ER-2 aircraft. *J. Atmos. Oceanic Technol.*, **13**, 795–809.
- Houze, R. A., F. D. Marks, Jr, and R. A. Black, 1992: Dual-aircraft investigation of the inner core of Hurricane Norbert. Part II: Mesoscale distribution of ice particles. *J. Atmos. Sci.*, **49**, 943-962.
- Jones, W. L., P.G. Black, V.E. Delnore, and C. T. Swift, 1981: Airborne microwave remote sensing measurements of Hurricane Allen. *Science*, **214**, 274-280.
- Jorgensen, D. P., 1984: Mesoscale and convective-scale characteristics of mature hurricanes. Part I: General observations by research aircraft. *J. Atmos. Sci.*, **41**, 1268–1286.
- \_\_\_\_\_, E. J. Zipser, and M. A. LeMone, 1985: Vertical motions in intense hurricanes. *J. Atmos. Sci.*, **42**, 839-856.
- \_\_\_\_\_, and P. T. Willis, 1982: A Z-R relationship for hurricanes. *J. Appl. Meteor.*, **21**, 356-366.
- Klazura, G. E., J. M. Thomale, D. S. Kelly, and P. Jendrowski, 1999: A comparison of NEXRAD WSR-88D radar estimates of rain accumulation with gauge measurements for high- and low-reflectivity horizontal gradient precipitation events. *J. Atmos. Oceanic Technol.*, **16**, 1842–1850.
- Marks, F. D., Jr., 1985: Evolution of the structure of precipitation in Hurricane Allen (1980). *Mon. Wea. Rev.*, **113**, 909–930.
- \_\_\_\_\_, D. Atlas, and P. T. Wills, 1993: Probability-matched reflectivity-rainfall relations for a hurricane from aircraft observations. *J. Appl. Meteor.*, **32**, 1134-1141.
- \_\_\_\_\_, and R. A. Houze, 1987: Inner core structure of Hurricane Alicia from airborne Doppler radar observations. *J. Atmos. Sci.*, **32**, 1134-1141.
- Merceret, F., 1974: On the size distribution of raindrops in Hurricane Ginger. *Mon. Wea. Rev.*, **102**, 714-716.
- Molinari, J., P. Moore, and V. Idone, 1999: convective structure of hurricanes as revealed by lightning locations. *Mon. Wea. Rev.*, **127**, 520-534.
- Olsen, R. L., D. V. Rogers, and D. B. Hodge, 1978: The  $aR^b$  relation in the calculation of rain attenuation. *IEEE Trans. Antennas Propagat.*, **AP-26**, 318-329.

- Oury, S., J. Testud, and V. Marecal, 1999: Estimate of precipitation from the dual-beam airborne radars in TOGA COARE. Part 1: The K-Z relationships derived from stereo and quad-beam analysis. *J. Appl. Meteor.*, **38**, 156–174.
- Pruppacher, H. R., and J. D. Klett, 1997: *Microphysics of clouds and precipitation*. Kluwer Academic Publishers, 954 pp.
- Rodgers, R. R., and M. K. Yau, 1989: *A short course in cloud physics*. Butterworth-Heinemann, 290 pp.
- Ryde, J. W., 1947: The attenuation and radar echoes produced at centimeter wavelengths by various meteorological phenomena. *Meteorological Factors in Radio Wave Propagation*, Physical Society of London, 169-189.
- Schumacher, C., and R. A. Houze, 2000: Comparison of radar data from the TRMM satellite and Kwajalein oceanic validation site. *J. Appl. Meteor.*, **39**, 2151–2164.
- Smith, J. A., M. L. Baeck, Y. Zhang, and C. A. Doswell, 2001: Extreme rainfall and flooding from supercell thunderstorms. *Journal of Hydrometeorology*, **2**, 469–489.
- Steiner, M., R. A. Houze, and S. E. Yuter, 1995: Climatological characterization of three-dimensional storm structure from operational radar and rain gauge data. *J. Appl. Meteor.*, **34**, 1978–2007.
- Stephens, G., 1994: *Remote sensing of the lower atmosphere*. Oxford University Press, 523 pp.
- Stout, G. E., and E. A. Mueller, 1968: Survey of relationships between rainfall rate and radar reflectivity in the measurement of precipitation. *J. Appl. Meteor.*, **7**, 465–474.
- Swift, C. T., D. C. Dehority, A. B. Tanner, and R. E. McIntosh, 1986: Passive microwave spectral emission from saline ice at C-band during the growth phase. *IEEE Trans. Geosci. Remote Sens.*, **GE-24**, 840-848.
- Szoke, E. J., and E. J. Zipser, 1986: A radar study of convective cells in mesoscale systems in GATE. Part II: Life cycles of convective cells. *J. Atmos. Sci.*, **43**, 199–218.
- \_\_\_\_\_, \_\_\_\_\_, and D. P. Jorgensen, 1986: A radar study of convective cells in mesoscale systems in GATE. Part I: Vertical profile statistics and comparison with Hurricanes. *J. Atmos. Sci.*, **43**, 182–198.
- Tanner, A., C. T. Swift, and P. G. Black, 1987: Operational airborne remote sensing of wind speeds in hurricanes. Preprints, *17<sup>th</sup> Conf. Hurricane and Tropical Meteorology*, Miami, FL, Amer. Meteor. Soc., 385-387.

- Uhlhorn, E. W., and P. G. Black, 2003: Verification of remotely sensed sea surface winds in hurricanes. *J. Atmos. Oceanic Technol.*, **20**, 99-116.
- Wexler, R., and D. Atlas, 1963: Radar reflectivity and attenuation of rain. *J. Appl. Meteor.*, **2**, 276-280.
- Wilheit, T. T., A. T. C. Chang, Rao M. S. V., E. B. Rodgers, and J. S. Theon, 1977: A satellite technique for quantitatively mapping rainfall rates over the oceans. *J. Appl. Meteor.*, **16**, 551-560.
- Willis, P. L., and D. P. Jorgensen, 1981: Reflectivity relationships for hurricanes. Preprints, *20<sup>th</sup> Conf. on Radar Meteorology*, Boston, MA, Amer. Meteor. Soc., 199-200.
- Yuter, S. E., and R. A. Houze, Jr., 1995: Three-dimensional kinematic and microphysical evolution of Florida cumulonimbus. Part II: Frequency distributions of vertical velocity, reflectivity, and differential reflectivity. *Mon. Wea. Rev.*, **123**, 1941-1963.
- Zipser, E. J., and K. R. Lutz, 1994: The vertical profile of radar reflectivity of convective cells: A strong indicator of storm intensity and lightning probability? *Mon. Wea. Rev.*, **122**, 1751-1759.

## **List of Tables:**

Table 1. Characteristics of Hurricane Bonnie and Humberto flights

Table 2. Correlation coefficients and best fit equations for different sample sets from least square regressions between SFMR and radar rain rates.

Table 3. Comparison of original SFMR retrieved and b-coefficient corrected SFMR rain rates at a set of K values at the highest frequency (7.22 GHz) of SFMR.

Table 4. Mean errors and best fit equations for different sample sets from least square regressions between SFMR corrected rain rates and radar rain rates (correlation coefficients are as same as in Table 2)

Table A1. Statistics of the bias of TA corrected reflectivity according to EDOP (EDOP-TA Corrected) at mean and selected percentile levels (in dB)

## List of Figures:

Figure 1. Geographic locations of SFMR/radar co-located rain rate measurements used in this study. Flight tracks are indicated by solid line and storm centers during the time period of paired samples are indicated by (\*). Storm names related to each flight are printed in the figure.

Figure 2. SFMR-LF and SFMR-TA rain rate comparisons for all samples. The solid line indicates perfect correlation and the dashed line indicates the best fit. Correlation coefficients are indicated.

Figure 3. Rainfall attenuation coefficient  $K$  ( $Np\ km^{-1}$ ) plotted as a function of rain rate ( $mm\ h^{-1}$ ) with the new exponent  $b=1.15$  (see text for detail).

Figure 4. SFMR-LF and SFMR-TA rain rate comparisons for all samples after SFMR algorithm correction. The solid line indicates perfect correlation and the dashed line indicates the best fit. Mean rain rates ( $mm\ h^{-1}$ ) and correlation coefficients are indicated.

Figure 5. Probability density functions (PDF) of SFMR rain rate errors relative to TA rain rate (solid line), PDF of SFMR rain rate errors relative to LF rain rate (dot line), cumulative density function (CDF) of the SFMR rain rate errors relative to TA rain rate (dash line) and CDF of SFMR rain rate errors relative to LF rain rate (dash dot line) for all samples. For the  $n=820$  observations, mean errors and standard deviations are indicated in the upper left corner of the figure.

Figure 6. Probability density functions (PDF) of SFMR rain rate errors ( $SFMR - TA$ ) for stratiform samples (solid line) and convective samples (dot line) and cumulative density function (CDF) of the SFMR rain rate errors for stratiform samples (dash line) and convective samples (dash dot line). Mean errors and standard deviations for these two sample subsets are indicated in the upper left corner of the figure.

Figure 7. SFMR rain rate error relative to TA radar rain rate plotted as a function of TA rain rate ( $\text{mm h}^{-1}$ ) for (a) stratiform samples; (b) convective samples. Linear regressions (dash lines) and correlation coefficients (R) are indicated.

Figure 8. Same as in Fig. 7, but x-axis represents SFMR wind speed ( $\text{m s}^{-1}$ ).

Figure 9. Same as in Fig. 7, but x-axis represents normalized radial distance ( $r/r_0$ ).

Figure 10. The retrieved versus true path-integrated (mean) rain rate over the whole rain column for different conditions: (a) the separate effects due to the freezing level = 4.5 km (dot line),  $\text{rain\_above} = \text{rain\_below} - 5 \text{ mm h}^{-1}$  (dash line), and  $\text{rain\_above} = \text{rain\_below} + 5 \text{ mm h}^{-1}$  (dash dot line, see text for details); (b) the combination effects due to the freezing level = 4.5 km and  $\text{rain\_above} = \text{rain\_below} - 5 \text{ mm h}^{-1}$  (dash line), and the freezing level = 4.5 km and  $\text{rain\_above} = \text{rain\_below} + 5 \text{ mm h}^{-1}$  (dash dot line). The 1:1 line is indicated.

Figure A1. Probability density functions (PDFs) and cumulative density function (CDFs) of the EDOP reflectivity and TA corrected reflectivity (+6.0 dB) during Hurricane Bonnie flights during Aug. 24 and 26, 1998.

Figure A2. Probability density functions (PDFs) and cumulative density function (CDFs) of the EDOP reflectivity and TA corrected reflectivity (+4.5 dB) during one Hurricane Humberto flight leg around 21:40 UTC on Sept. 23, 2001.

Table 1. Characteristics of Hurricane Bonnie and Humberto flights

Flight	Time (UTC)	Storm	Altitude (km)	Number of paired samples	Percentage of paired samples classified as stratiform	Percentage of paired samples classified as convective	SFMR wind maximum ( $\text{m s}^{-1}$ )
980824-I1	19:58-25:29	Bonnie	1.5	475	74% (353)	26% (122)	46
980826-I1	18:00-23:10	Bonnie	2.1	85	66% (56)	34% (29)	42
010923-I1	20:03-24:00	Humberto	1.8	110	52% (57)	48% (53)	43
010924-I1	20:52-25:01	Humberto	1.8	150	65% (97)	35% (53)	34

Table 2. Correlation coefficients and best fit equations for different sample sets from least square regressions between SFMR and radar rain rates.

	SFMR vs. LF		SFMR vs. TA	
	Correlation coefficient	Best fit equation	Correlation coefficient	Best fit equation
All samples (820 samples)	0.82	SFMR= 4.92+0.6(LF)	0.82	SFMR= 4.16+0.65(TA)
Bonnie (560 samples)	0.81	SFMR= 5.11+0.54(LF)	0.82	SFMR= 3.83+0.65(TA)
Humberto (260 samples)	0.84	SFMR= 5.68+0.63(LF)	0.81	SFMR= 5.07+0.62(TA)
Stratiform (563 samples)	0.77	SFMR= 4.75+0.58(LF)	0.77	SFMR= 3.73+0.68(TA)
Convective (257 samples)	0.79	SFMR= 6.88+0.54(LF)	0.77	SFMR= 5.40+0.59(TA)

Table 3. Comparison of original SFMR retrieved and b-coefficient corrected SFMR rain rates at a set of K values at the highest frequency (7.22 GHz) of SFMR.

K at 7.22 GHz (Np km <sup>-1</sup> )	0.00388	0.01165	0.03555	0.06881	0.11033	0.15946	0.21573
Original SFMR rain rate (mm h <sup>-1</sup> )	5.00	10.00	20.00	30.00	40.00	50.00	60.00
Corrected SFMR rain rate (mm h <sup>-1</sup> )	6.13	13.33	28.90	45.38	62.48	80.03	97.95

Table 4. Mean errors and best fit equations for different sample sets from least square regressions between SFMR corrected rain rates and radar rain rates (correlation coefficients are as same as in Table 2)

	SFMR vs. LF		SFMR vs. TA	
	Mean Error (mm h <sup>-1</sup> )	Best fit equation	Mean Error (mm h <sup>-1</sup> )	Best fit equation
All samples (820 samples)	5.05	SFMR=5.45+0.97(LF)	4.74	SFMR=4.22+1.04(TA)
Bonnie (560 samples)	4.18	SFMR=5.93+0.85(LF)	4.31	SFMR=3.92+1.03(TA)
Humberto (260 samples)	6.91	SFMR=6.54+1.03(LF)	5.67	SFMR=5.54+1.01(TA)
Stratiform (563 samples)	4.45	SFMR=5.37+0.91(LF)	4.47	SFMR=3.75+1.07(TA)
Convective (257 samples)	6.34	SFMR=8.33+0.88(LF)	5.32	SFMR=5.89+0.97(TA)

Table A1. Statistics of the bias of TA corrected reflectivity according to EDOP (EDOP-TA Corrected) at mean and selected percentile levels (in dB)

	Bonnie	Humberto
Mean	+0.73	+0.52
10%	+1.28	+0.99
30%	+1.47	+1.71
50%	+0.47	+0.64
70%	-0.08	-0.37
90%	+0.29	+0.43

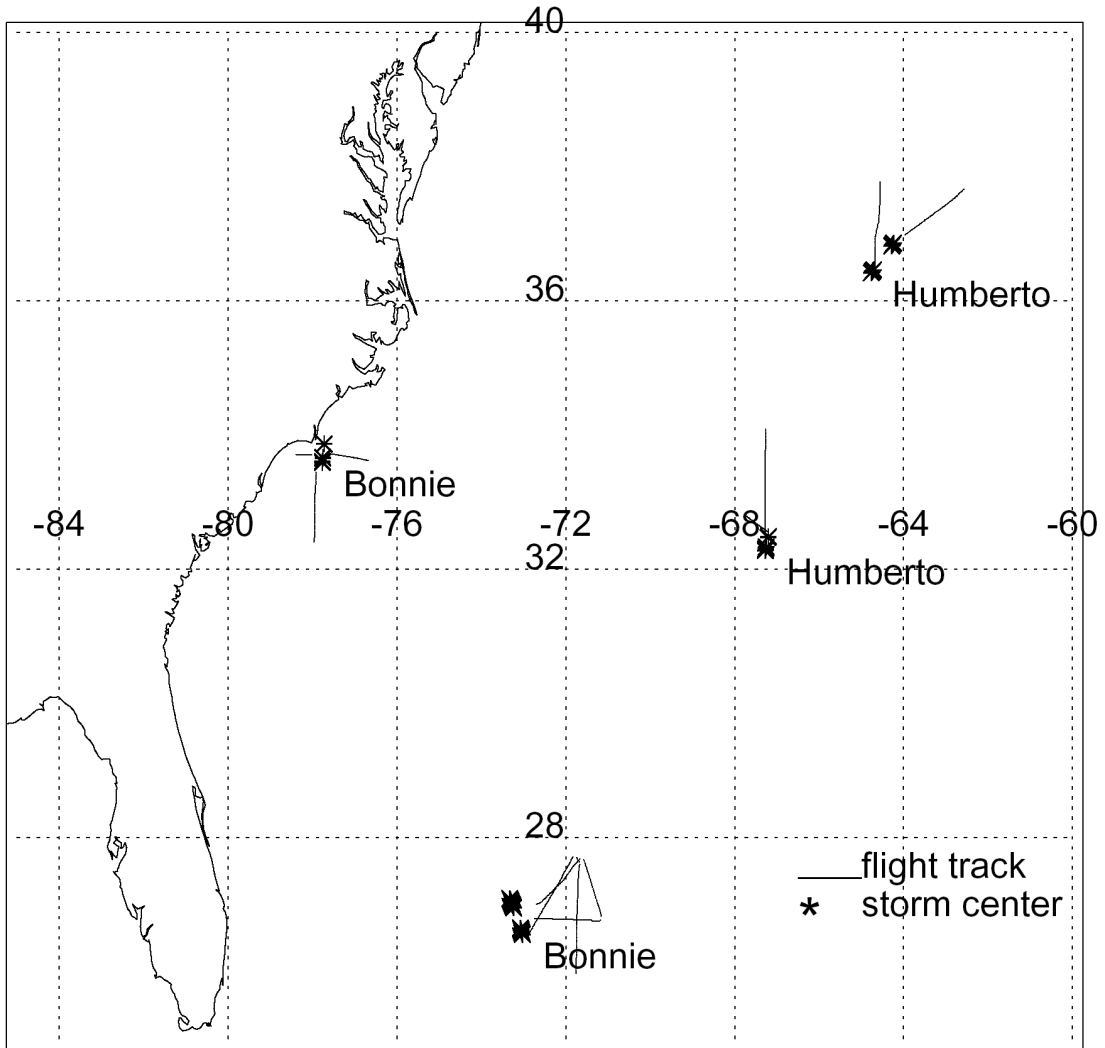


Figure 1. Geographic locations of SFMR/radar co-located rain rate measurements used in this study. Flight tracks are indicated by solid line and storm centers during the time period of paired samples are indicated by (\*). Storm names related to each flight are printed in the figure.

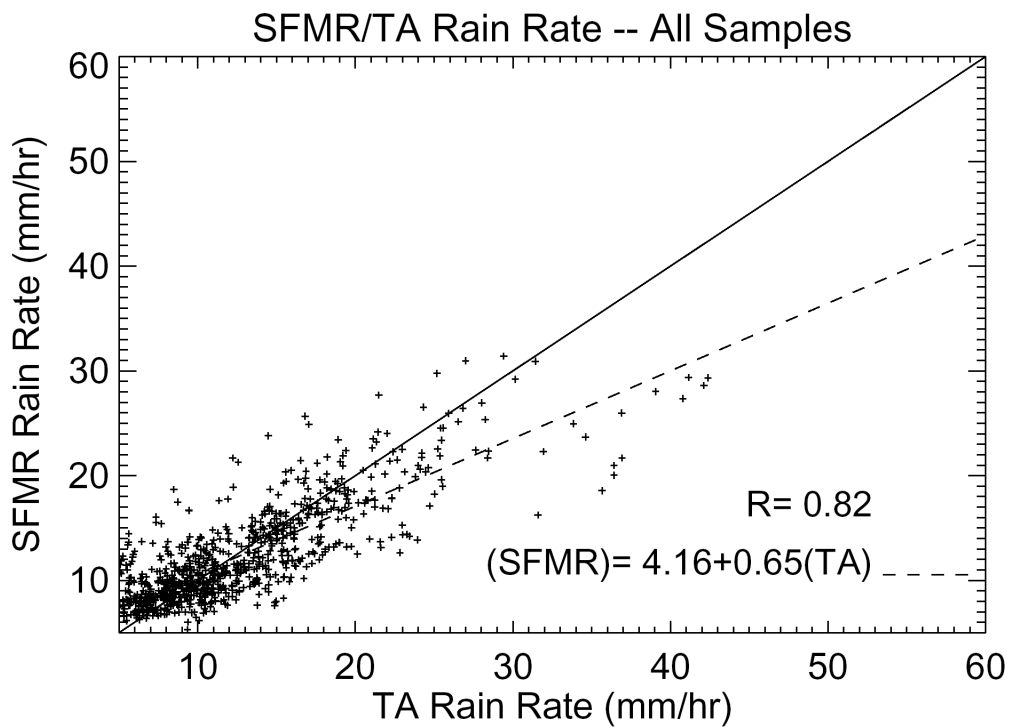
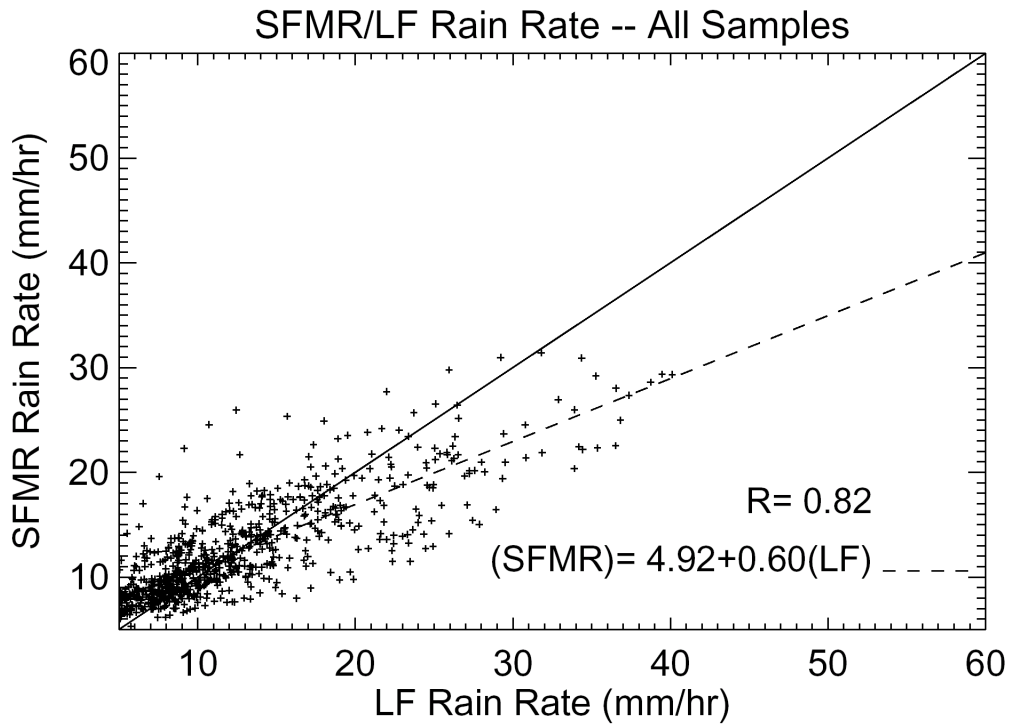


Figure 2. SFMR-LF and SFMR-TA rain rate comparisons for all samples. The solid line indicates perfect correlation and the dashed line indicates the best fit. Correlation coefficients are indicated.

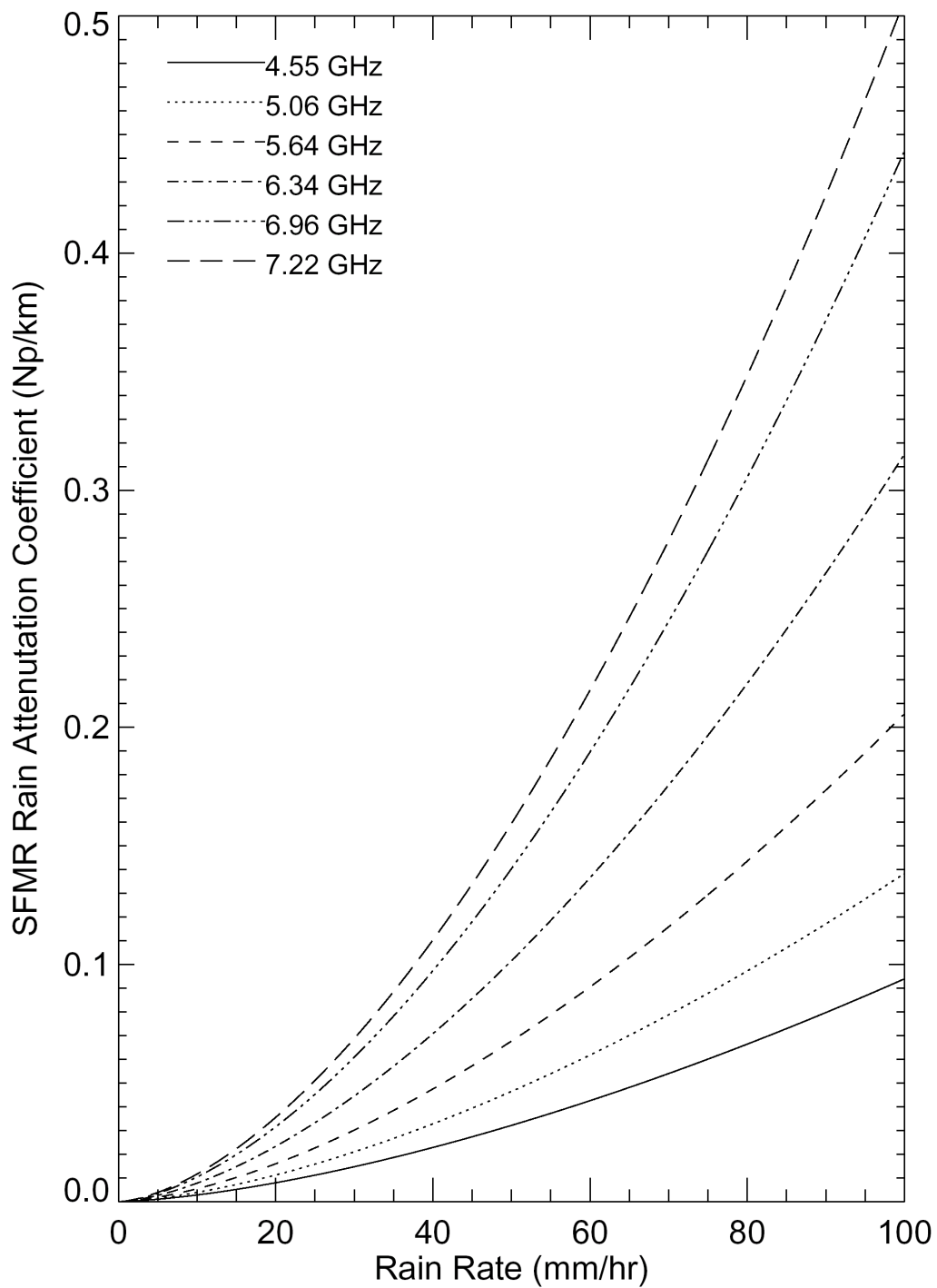


Figure 3. Rainfall attenuation coefficient  $K$  ( $Np\ km^{-1}$ ) plotted as a function of rain rate ( $mm\ h^{-1}$ ) with the new exponent  $b=1.15$  (see text for detail).

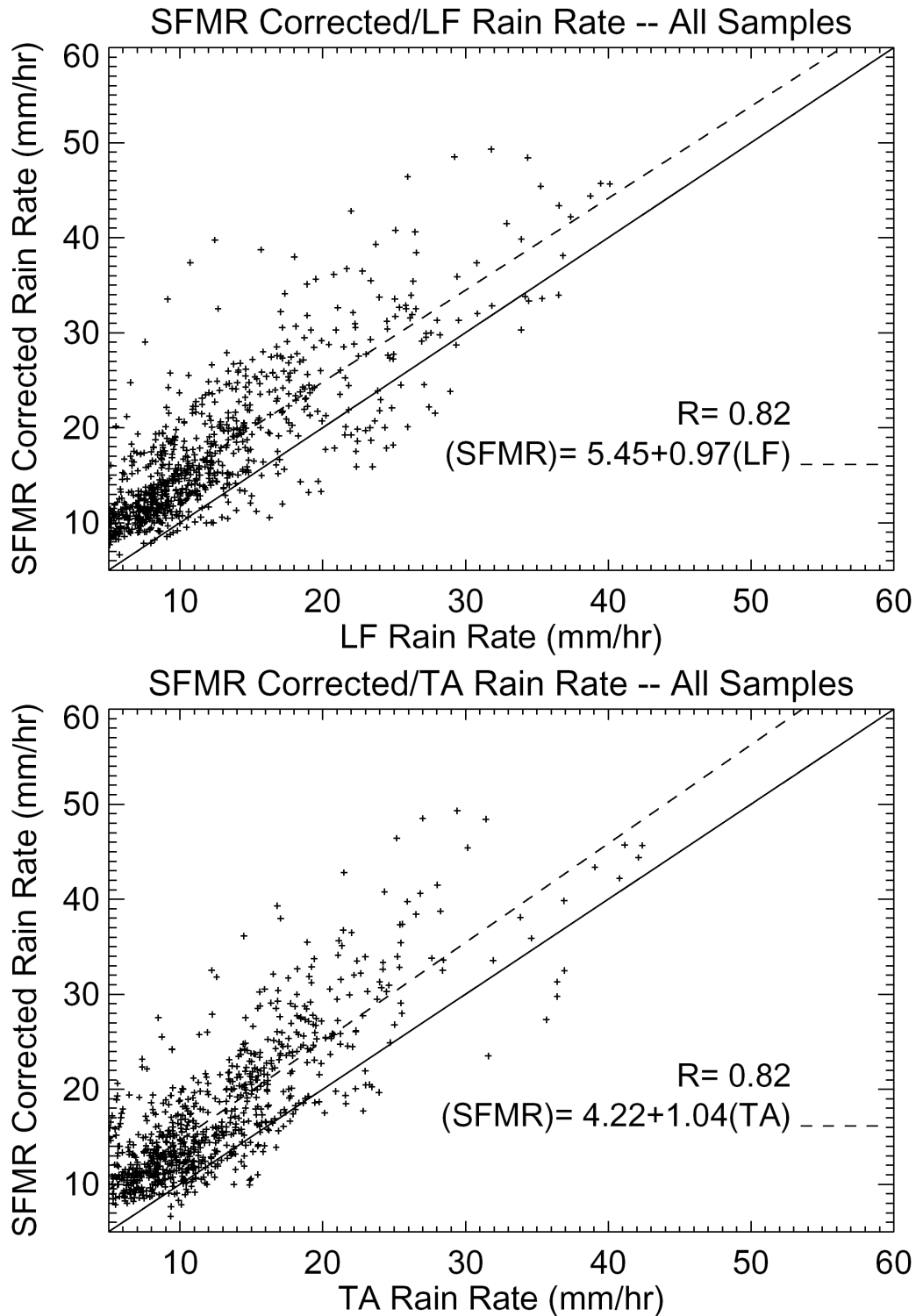


Figure 4. SFMR-LF and SFMR-TA rain rate comparisons for all samples after SFMR algorithm correction. The solid line indicates perfect correlation and the dashed line indicates the best fit. Mean rain rates ( $\text{mm h}^{-1}$ ) and correlation coefficients are indicated.

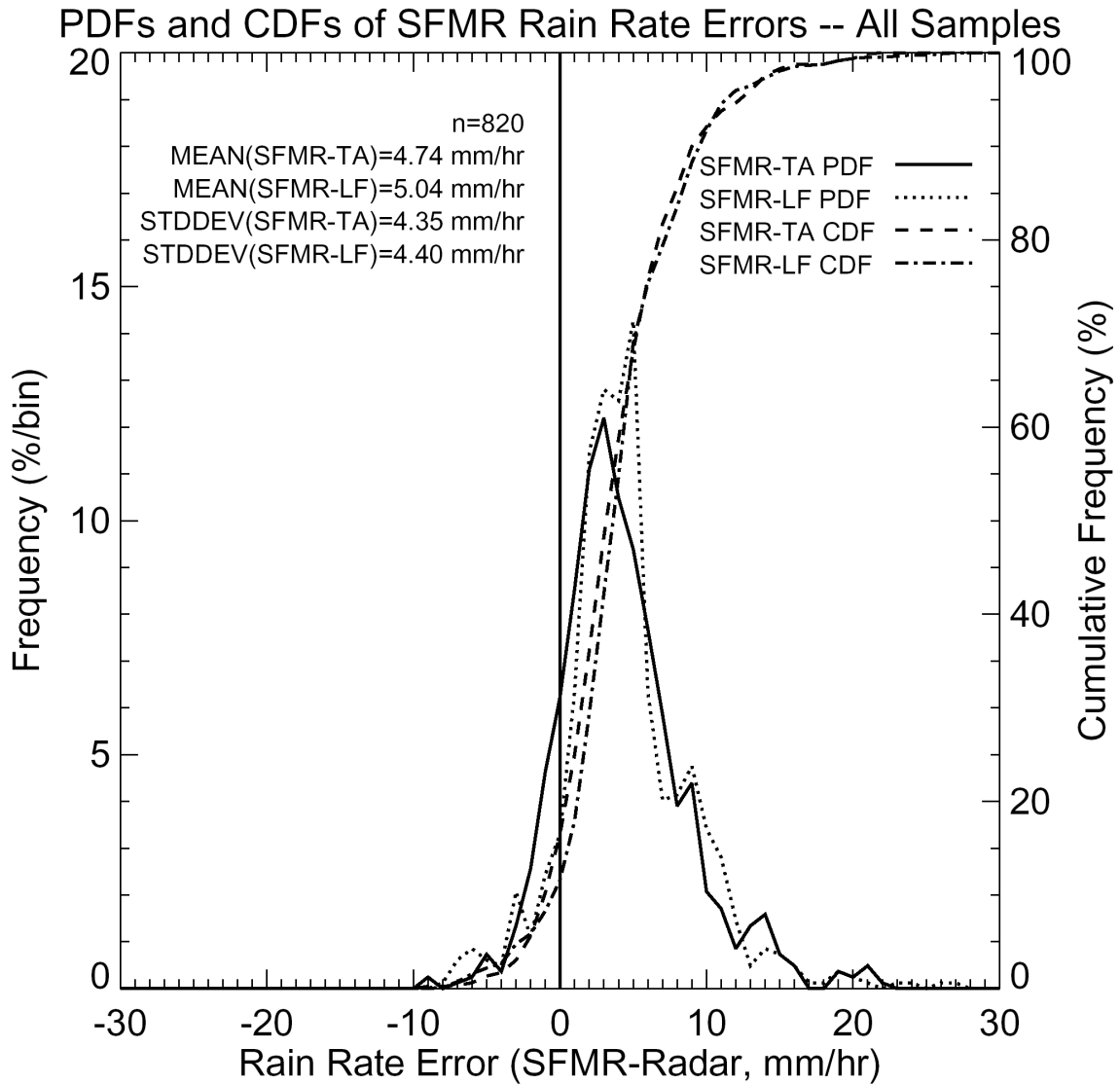


Figure 5. Probability density functions (PDF) of SFMR rain rate errors relative to TA rain rate (solid line), PDF of SFMR rain rate errors relative to LF rain rate (dot line), cumulative density function (CDF) of the SFMR rain rate errors relative to TA rain rate (dash line) and CDF of SFMR rain rate errors relative to LF rain rate (dash dot line) for all samples. For the n=820 observations, mean errors and standard deviations are indicated in the upper left corner of the figure.

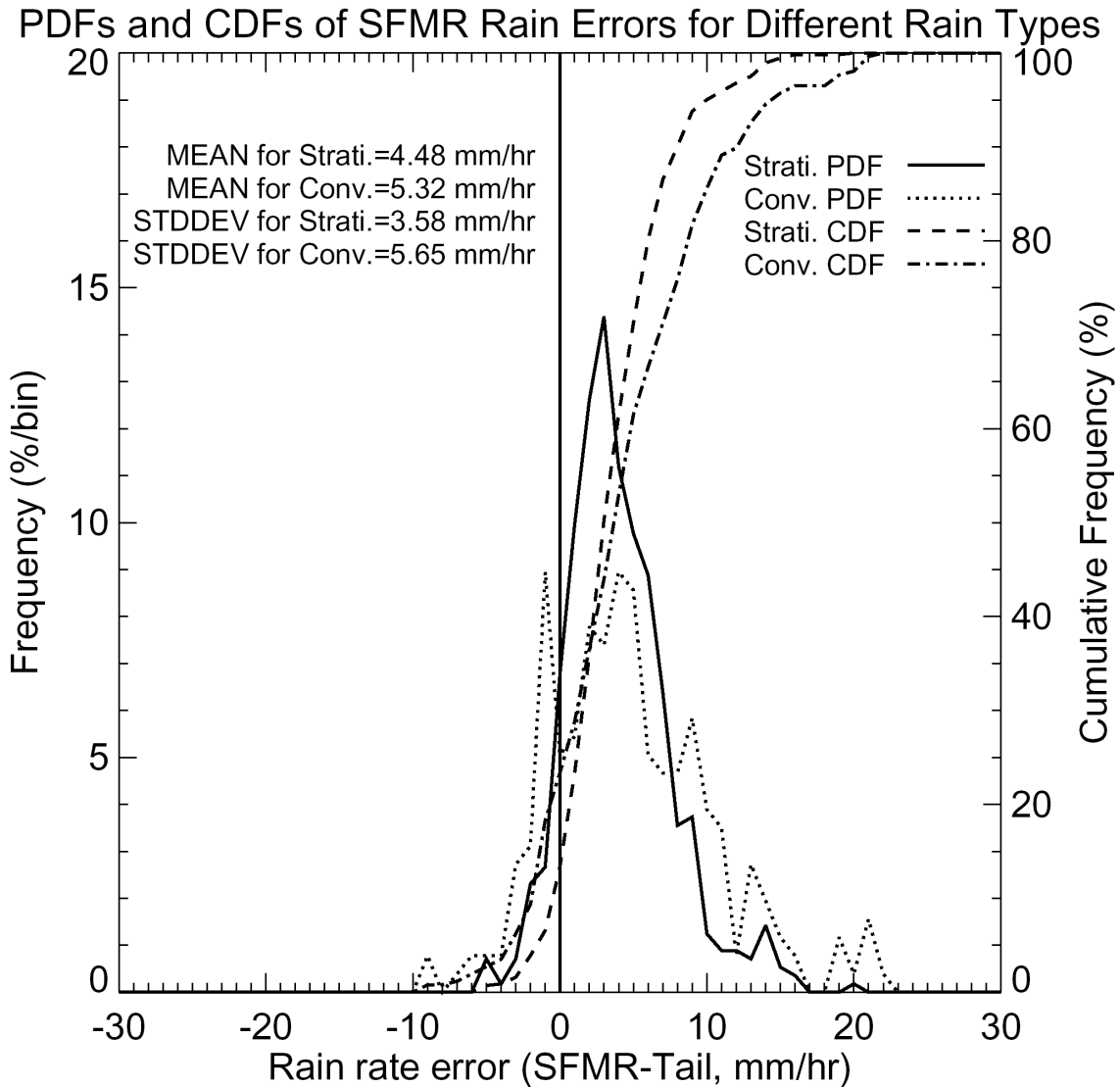


Figure 6. Probability density functions (PDF) of SFMR rain rate errors (SFMR – TA) for stratiform samples (solid line) and convective samples (dot line) and cumulative density function (CDF) of the SFMR rain rate errors for stratiform samples (dash line) and convective samples (dash dot line). Mean errors and standard deviations for these two sample subsets are indicated in the upper left corner of the figure.

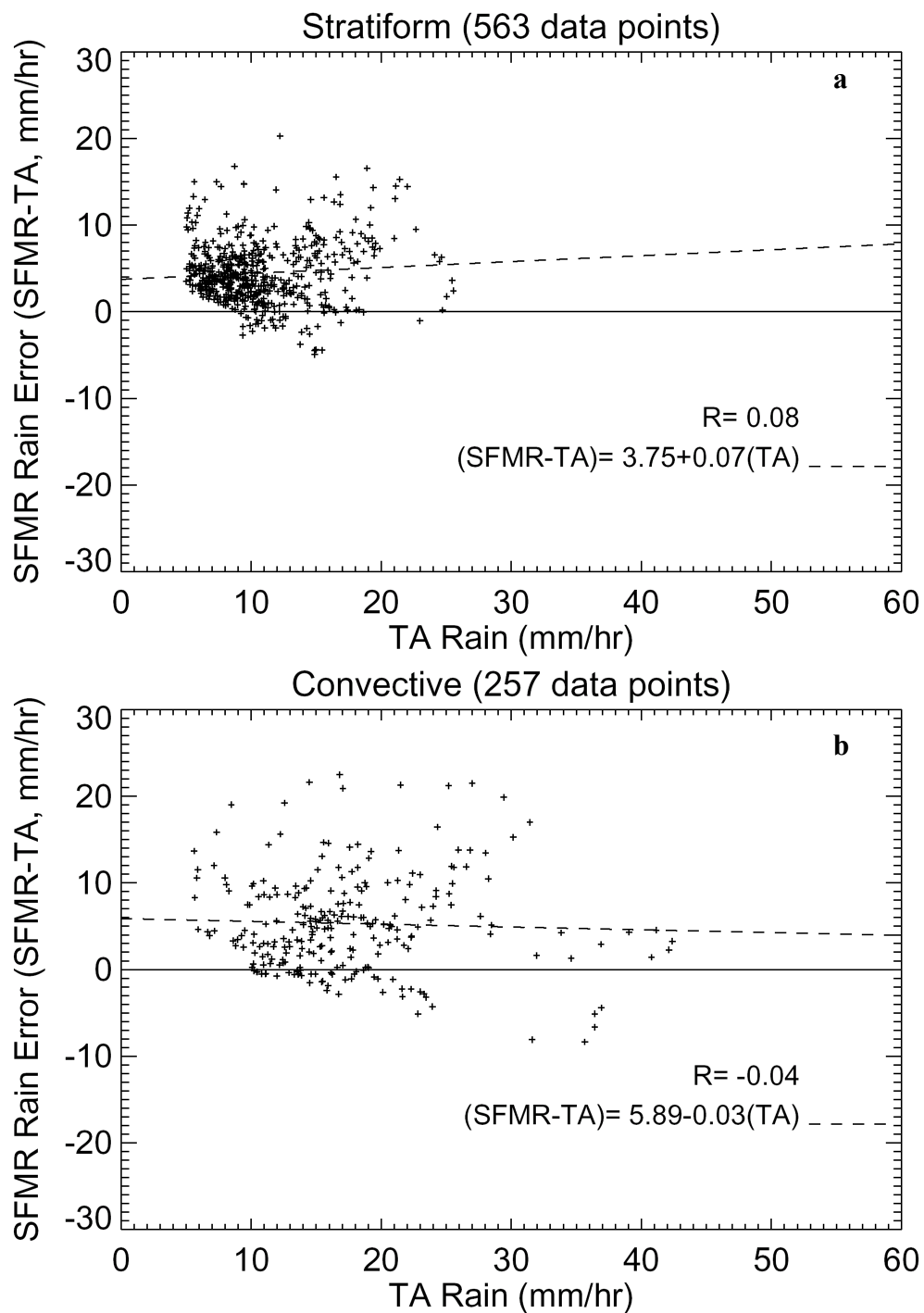


Figure 7. SFMR rain rate error relative to TA radar rain rate plotted as a function of TA rain rate ( $\text{mm h}^{-1}$ ) for (a) stratiform samples; (b) convective samples. Linear regressions (dash lines) and correlation coefficients (R) are indicated.

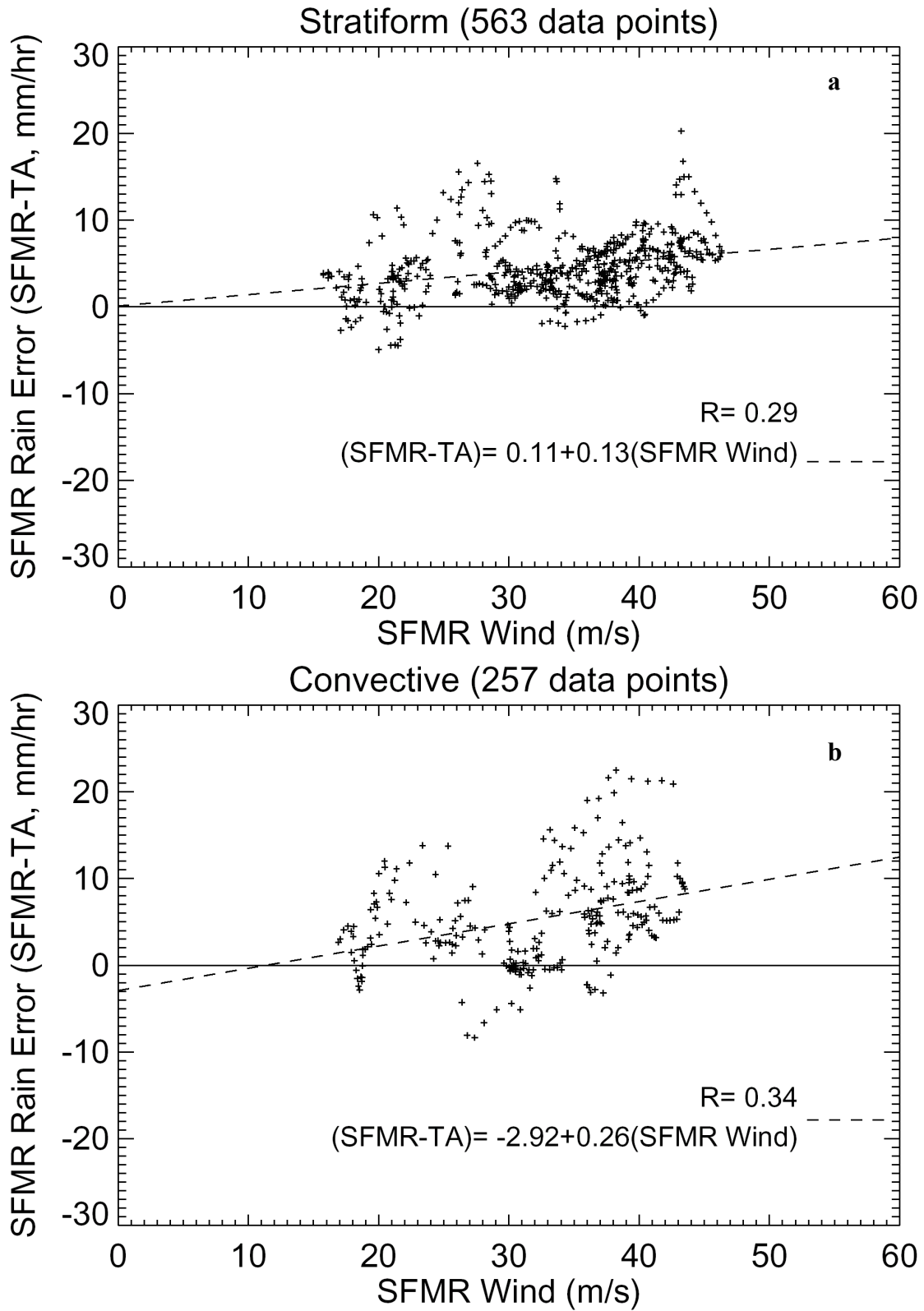


Figure 8. Same as in Fig. 7, but x-axis represents SFMR wind speed ( $\text{m s}^{-1}$ ).

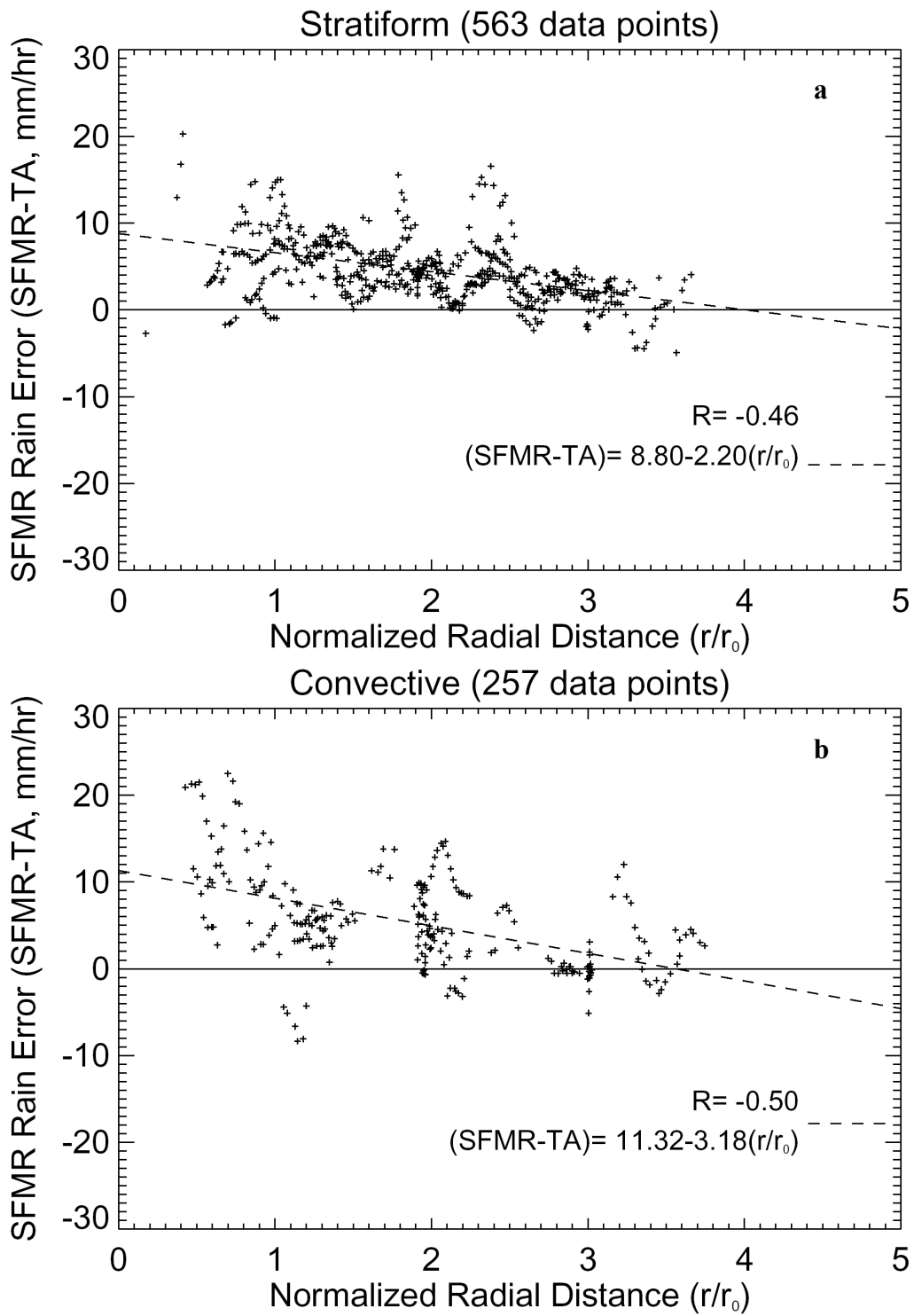


Figure 9. Same as in Fig. 7, but x-axis represents normalized radial distance ( $r/r_0$ ).

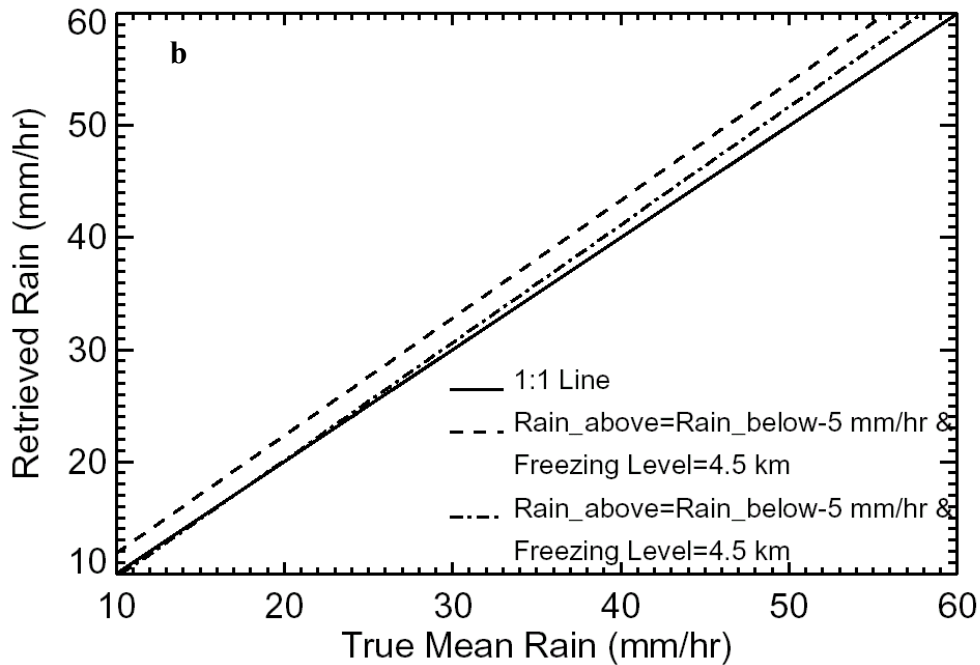
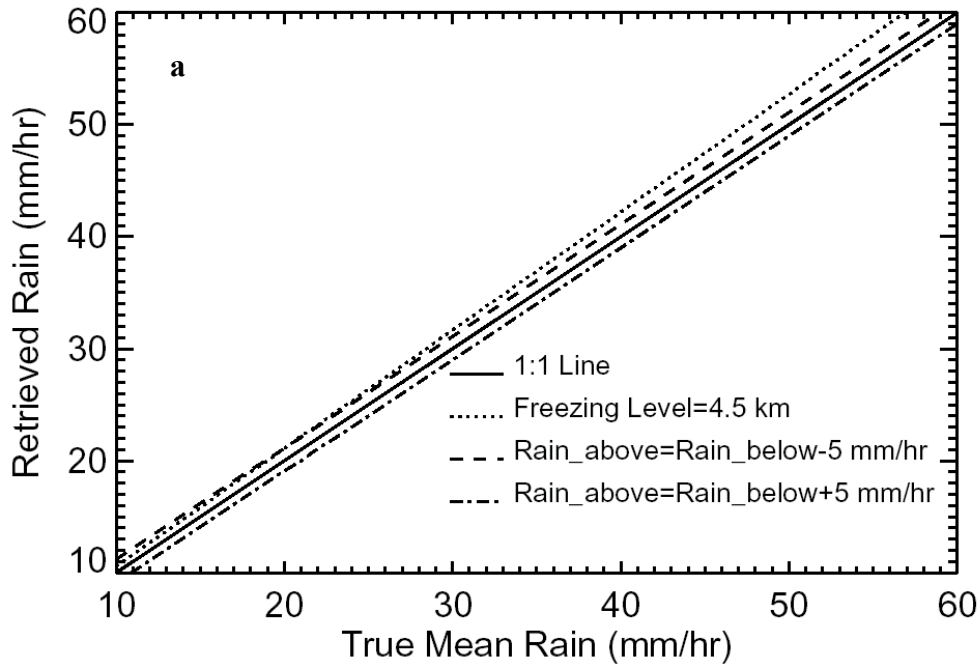


Figure 10. The retrieved versus true path-integrated (mean) rain rate over the whole rain column for different conditions: (a) the separate effects due to the freezing level = 4.5 km (dot line),  $rain\_above = rain\_below - 5\text{ mm h}^{-1}$  (dash line), and  $rain\_above = rain\_below + 5\text{ mm h}^{-1}$  (dash dot line, see text for details); (b) the combination effects due to the freezing level = 4.5 km and  $rain\_above = rain\_below - 5\text{ mm h}^{-1}$  (dash line), and the freezing level = 4.5 km and  $rain\_above = rain\_below + 5\text{ mm h}^{-1}$  (dash dot line). The 1:1 line is indicated.

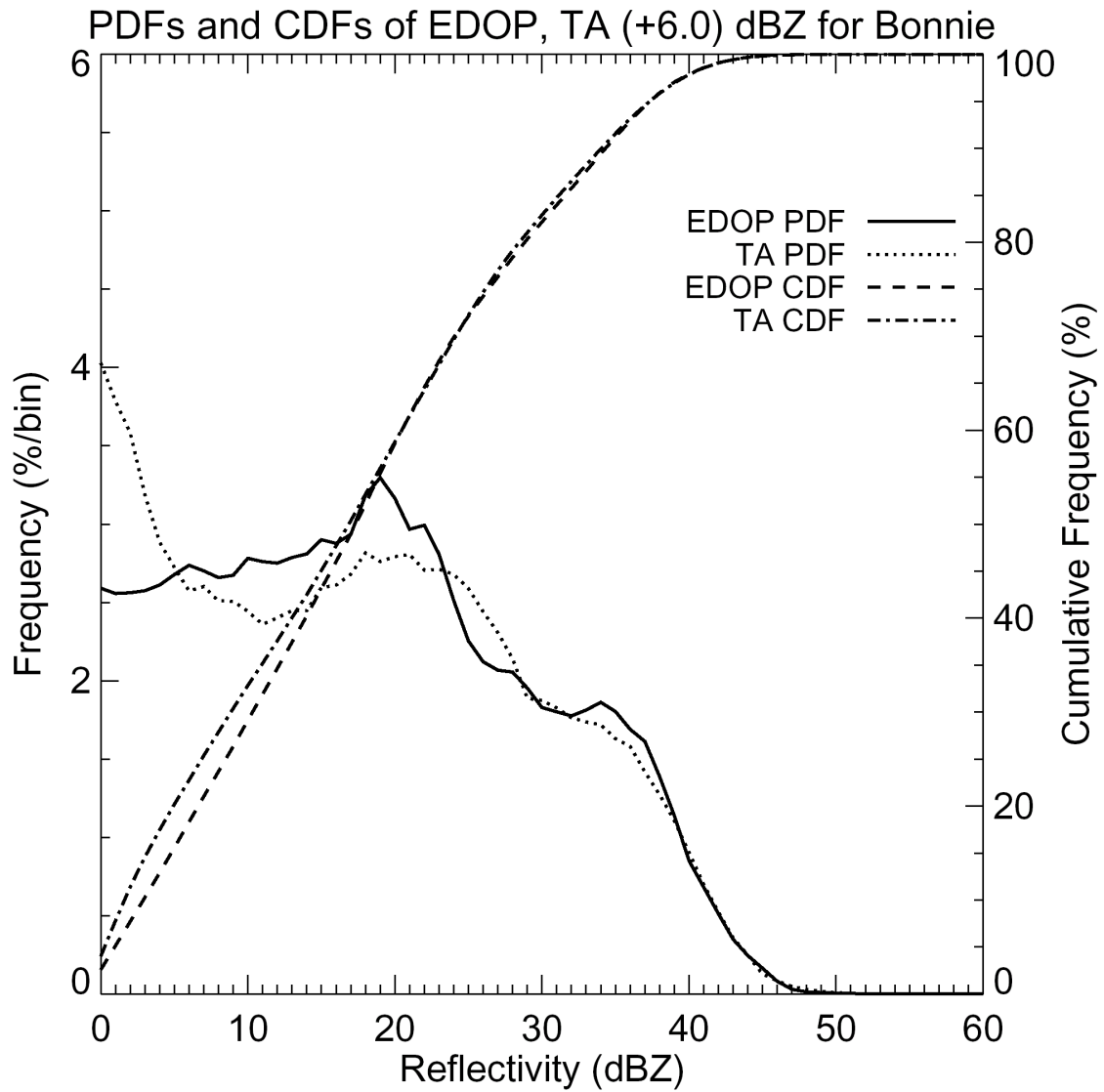


Figure A1. Probability density functions (PDFs) and cumulative density function (CDFs) of the EDOP reflectivity and TA corrected reflectivity (+6.0 dB) during Hurricane Bonnie flights during Aug. 24 and 26, 1998.

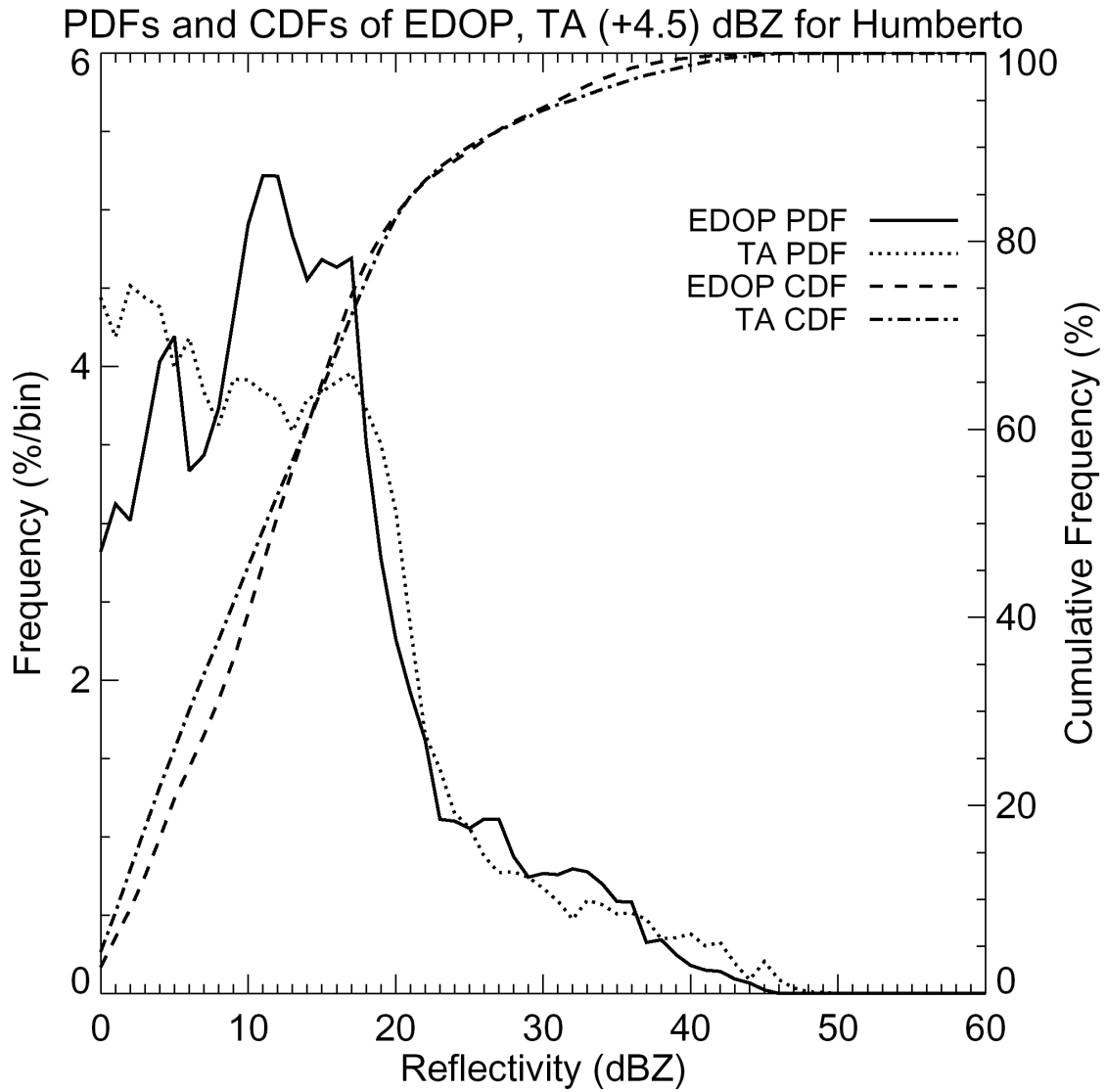


Figure A2. Probability density functions (PDFs) and cumulative density function (CDFs) of the EDOP reflectivity and TA corrected reflectivity (+4.5 dB) during one Hurricane Humberto flight leg around 21:40 UTC on Sept. 23, 2001.